Energetic particle mode stability in tokamaks with hollow *q*-profiles

F. Zonca,[a] S. Briguglio, L. Chen,[b] S. Dettrick,[b] G. Fogaccia, D. Testa,[c] and G. Vlad
Associazione EURATOM-ENEA sulla Fusione, C.P. 65-00044 Frascati, Rome, Italy

(Received 11 July 2002; accepted 23 August 2002)

A thorough analysis of energetic particle modes (EPM) stability and mode structures is presented for tokamaks with hollow q profiles. Focusing on the region near the minimum-q surface, EPM gap modes and resonant EPMs are shown to exist as solutions of the same dispersion relation. By controlling the fast ion distribution function, or, equivalently, their fundamental dynamical properties, a smooth transition between these two classes of modes is obtained within the EPM dispersion relation. When toroidal coupling becomes important, it is demonstrated that EPMs may have either single or double hump radial structures. The local analyses of EPM stability and mode structures near the minimum-q surface are put in the broader framework of EPM stability and EPM induced transport in tokamaks with hollow q profiles and a brief summary is also given of present understanding of such problems based on results of three-dimensional nonlinear hybrid magneto–hydrodynamic–gyrokinetic simulations. Possible implications of present results are discussed in terms of experimental observations and possibilities of designing novel experimental setups to probe, at least conceptually, the complex predictions of theory. © *2002 American Institute of Physics.* [DOI: 10.1063/1.1519241]

I. INTRODUCTION

In this work, we discuss the properties of energetic particle modes (EPM)[1] excited by the presence of ICRH (ion cyclotron resonant heating) induced energetic ion tails[2,3] in tokamaks with hollow q profiles. Such equilibria are of particular interest in present experiments because of the improved confinement regimes that they make possible to achieve. From the point of view of EPM excitations, the plasma cross section is divided in three regions by the presence of the minimum-q surface. Inner and outer regions are obviously characterized by different values of magnetic shear and fast ion energy density. The plasma volume inside the minimum-q surface has typically negative and often small shear. Here, the fast ion energy density is maximum, due to the spatial localization of ICRH. Meanwhile, the outer region has positive magnetic shear but small fast ion energy density, since this is where ICRH power density is smallest. A toroidal annulus, centered at the minimum-q surface, separates these two regions and is characterized by peculiar properties of both EPM stability and mode structures. For a wave of toroidal mode number n, the width of the annulus is given by the inequality $s^2 \lesssim S^2/n$. Here, $s \equiv rq'/q$ is the conventional definition of magnetic shear, ''prime'' denotes derivation in the radial direction r and $S^2 \equiv r_0^2 q''(r_0)/q_0^2$ is a measure of the concavity of the q profile at the radial location of the minimum-q surface, where $r=r_0$, $q=q_0$, and $s \to 0$. This definition of the width of the toroidal annulus, that may appear obvious for $n=1$, has nontrivial reasons that are discussed in Sec. III.

For $s \gtrsim 1$, typical of the outer region, previous theories may be used to analyze EPM stability and mode structures (cf., e.g., Refs. 1 and 4). However, this is the region of minor interest from the point of view of EPM excitation by ICRH because that is where the fast ion energy density is smallest. For this reason, we will not consider it further in the present paper.

Former analyses,[2,3] assuming small but finite magnetic shear, are evidently relevant for discussions of EPM stability and mode structures in the plasma volume inside the minimum-q surface and that part of the outer region where shear is small. More recent studies[5–7] have also dealt with EPM excitations in the toroidal annulus at r_0. Nonetheless, a coherent or ''unified'' picture, capable of addressing small but finite as well as vanishing shear is still lacking. Similarly, analogies and/or peculiar aspects of EPM excitations at different radial locations are not fully clarified.

In this paper, we discuss the relationship between EPMs that are resonantly driven in the small but finite shear region with those that are excited in the toroidal annulus at r_0. There are various relevant aspects in this problem involving both linear (Secs. II and III) and nonlinear physics issues (Sec. IV).

In Sec. II, we present a detailed stability analysis of EPMs excited near the minimum-q surface. There, we show that two branches of EPM exist at r_0: *EPM gap modes* and the usual *resonant EPMs*.[1] These modes are described by the same dispersion relation and, in fact, they are the same mode but with different dominant damping mechanisms. EPM gap modes, specifically, have been previously discussed[5–7] in relationship with resonantly excited Alfvén modes—recently named Alfvén cascades[8]—that have been observed in Joint European Torus (JET) reversed shear (RS) discharges.[6,7] The characteristic signature of Alfvén cascades is the variation of their frequency with time. More precisely, they are *upwards*

[a]Electronic mail: zonca@frascati.enea.it
[b]Also at Department of Physics and Astronomy, University of California, Irvine, CA 92697-4575.
[c]Also at Plasma Science and Fusion Center, Massachusetts Institute of Technology, Boston, MA.

frequency chirping modes,[6–9] whose frequency is closely related to the local frequency of the shear Alfvén continuous spectrum at the radial position where the safety factor q has a minimum. This point was shown first in Ref. 6, where it was also argued that a localized mode above the local maximum of the shear Alfvén continuum was possible only in the presence of an ICRH induced energetic ion tail, and that the upwards frequency chirp was due to the change in time of q_0. Therefore, Alfvén cascades can be interpreted as localized *EPM gap modes*, in the sense that their existence as weakly growing modes in the local (near the minimum-q magnetic surface) gap of the shear Alfvén continuous spectrum is due to the presence of the fast ion population. In fact, the condition for the existence of EPM gap modes is a threshold condition on the fast ion density, which turns out to be (to the lowest order) independent of both the mode frequency and the toroidal mode number.[6,7] In Sec. II, we demonstrate that, in general, two types of EPM gap modes may exist, one localized just above the local maximum of the shear Alfvén continuous spectrum and one just below its local minimum.[5] The two modes *may coexist*, and which mode is actually excited depends on the response (resonant and nonresonant) of the fast ions to the wave and on the details of fast ion orbits. The two branches are also characterized by opposite signature in frequency: the former are *upwards frequency chirping* modes, while the latter would be *chirping downwards* in frequency as q_0 drops. Here, we discuss the present results suggesting the interesting possibility of designing experimental operation scenarii in which either one of the two branches or both are excited by simply controlling the fast ion tail energy, e.g., acting on the density of the minority ion species.

In order to establish a closer link with previous treatments,[1–4] in Sec. II we discuss the relationship of *EPM gap modes* with the usual *resonant EPMs*. As anticipated above, we demonstrate that these modes are described by the same dispersion relation and that they are indeed the same mode but with different dominant damping mechanisms. In fact, resonant EPMs can be destabilized only when the fast ion drive is stronger than the *local continuum damping*, whereas EPM gap modes are excited when the drive overcomes *nonlocal continuum damping* (the local continuum damping being zero by definition). A smooth transition from the characteristic features of gap EPMs to resonant EPMs can be obtained by controlling the ICRH power density and/or the position of the resonant absorption layer.

We further discuss EPM mode structures near a minimum-q surface when toroidal effects become important.[5] In particular, we derive the generalization of the EPM gap mode dispersion relation[5,6] when the toroidal coupling to poloidal sidebands cannot be considered as a perturbation. In this sense, our result could be considered as the dispersion relation for resonantly excited toroidal Alfvén eigenmodes (TAE)[10] and for the EPM branch of TAEs[1,4] near a minimum-q surface. It is also demonstrated that, if the value of q_0 further drops after the EPMs reach the TAE frequency, *double EPM* structures may develop and that this fact is very likely connected with the disappearance of Alfvén cascades after reaching the TAE gap.[6,7]

All the characteristic features of EPM stability and mode structures at r_0, discussed in Sec. II, are enriched by further insights when viewed and compared with those of resonantly excited EPMs in the small but finite shear region near or within the minimum-q surface. In Sec. III, we analyze analogies and/or peculiar aspects of EPM excitations at different radial locations and provide a unified description of the problem by means of multiple spatial scale analyses. The whole approach, based on a simple physical argument, results in a single mathematical formulation that describes both the small and zero magnetic shear cases with the same equations. In this framework, we argue that the most unstable EPMs are typically excited at or near the radial location where the energetic particle drive is strongest. Here, we also provide a detailed discussion of qualitatively different EPM excitation scenarii that can be expected on the basis of linear theory. From the experimental point of view, we suggest ways for discriminating such different conditions.

Numerical simulations of nonlinear EPM dynamics, performed using a hybrid magnetohydrodynamic gyrokinetic code,[11,12] are presented in Sec. IV. There, it is demonstrated that two qualitatively different scenarii may occur from the point of view of energetic ion transport after resonant excitation of EPMs within the minimum-q surface and of EPM gap modes at r_0. Such results confirm the dynamic complexity of EPM excitations in tokamaks with hollow q profiles and show that they cannot be adequately described by spectrographic measurements at the plasma edge only. As discussed in Sec. IV, direct measurements of fast ion spatial and energy distribution functions along with radially resolved frequency spectra, possibly using reflectometry, are required to actually discriminate among the various cases.

The plan of the paper is as follows. Section II presents a discussion of EPM stability and mode structures close to a minimum-q surface. In Sec. III, analogies and/or peculiar features of resonant EPM excitations at different radial locations are analyzed and put in a single coherent framework. Section IV, meanwhile, is a study of the same problems from the perspective of nonlinear dynamics. Section V, finally, is devoted to discussions and conclusions. Most of the technical details are given in three appendixes.

II. THE PHYSICAL MODEL: EPM GAP MODES VS RESONANT EPMS

Consider modes localized near r_0, where q has a minimum given by q_0. Consider also a given toroidal mode number n and a poloidal mode number m such that the normalized parallel wave vectors $\Omega_{A,m} \equiv nq_0 - m < 0$ and $\Omega_{A,m-1} \equiv nq_0 - m + 1 > 0$. It is then readily demonstrated that the condition under which continuum damping is minimized is that with $-1/2 < \Omega_{A,m} < 0$ and $1/2 < \Omega_{A,m-1} < 1$. In fact, this is the condition under which there is a frequency gap between the (m,n) mode continuum, that has a local maximum at r_0, and the $(m-1,n)$ mode continuum, that has a local minimum at r_0 (cf. Fig. 1). In the high-n limit, it is possible to demonstrate that no global Alfvén modes (GAE)[13,14] exist near an extremum of the Alfvén continuum. In fact, GAE exist as global eigenmodes within a radial potential well due

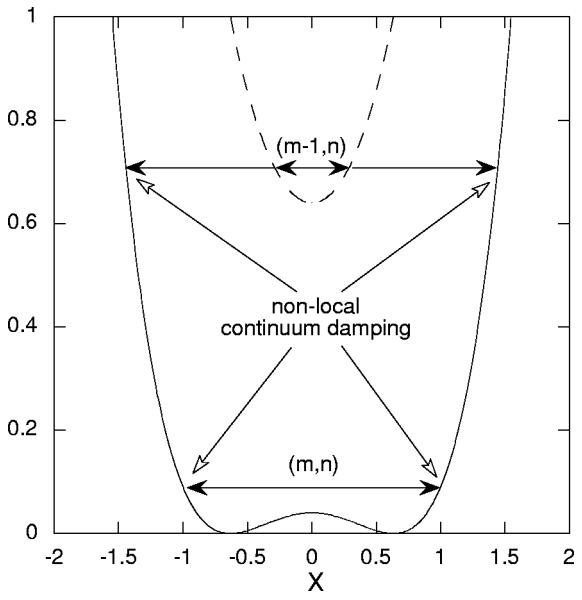

FIG. 1. Radial structure of the shear Alfvén continuous spectrum for the (m,n) and $(m-1,n)$ modes in the case $r_0/R_0 \ll \Omega_{A,m}+\Omega_{A,m-1} \leqslant 1$. The value of $q^2R_0^2k_{\|m,n}^2$ is shown vs $x \equiv \sqrt{nq_0''}(r-r_0)$. The frequencies of the (m,n) and $(m-1,n)$ modes are also shown as they are expected from Eq. (3).

to the effect of equilibrium current, which scales as $1/n$. In the presence of a fast ion population this *radial localization* effect may be provided by the energetic particles.[6] To show this, we start from Eq. (23) of Ref. 3 that, for the (m,n) mode reads

$$(e_\theta - e_{\mathbf{r}}\xi)\cdot\left[\Omega^2-\Omega_{A,m}^2\left(1+\frac{x^2}{\Omega_{A,m}}+\frac{x^4}{4\Omega_{A,m}^2}\right)\right] \times(e_\theta - e_{\mathbf{r}}\xi)\,\delta\psi_m+\Lambda_m\delta\psi_m=0, \tag{1}$$

where $e_{\mathbf{r}}$ and e_θ are, respectively, the radial and poloidal unit vectors, $\Omega \equiv \omega/\omega_A$, $\omega_A = v_A/qR_0$, v_A is the Alfvén speed, R_0 is the tokamak major radius, $x^2 = nq_0''(r-r_0)^2$, $\xi \equiv (i/n^{1/2})S(\partial/\partial x)$ with $S \equiv \sqrt{r_0^2q_0''/q_0^2}$, $\delta\psi_m$ is the mth poloidal harmonic of the scalar field perturbation and a similar equation can be written for the $(m-1,n)$ mode. The term Λ_m in Eq. (1) represents the fast ion contribution, whose nonresonant response can be approximated as[3]

$$\Lambda_m \simeq -\frac{q^2R_0^2}{k_\theta^2}\frac{4\pi\omega}{c^2}\frac{e_H^2}{m_H}\frac{2}{\pi}\int_0^\infty \frac{dz}{1+z^2}\overline{\langle J_0^2(\lambda_H)QF_{0H}\rangle}, \tag{2}$$

when the fast ion toroidal precession frequency, $\overline{\omega}_{dH}$, is such that $\overline{\omega}_{dH} \gg \omega$.[6,7] Here, integration in z accounts for the *nonlocal* response of fast ions due to finite Larmor orbit width. Meanwhile, $\overline{(\cdots)}$ indicates magnetic flux surface averaging, $\langle\cdots\rangle$ denotes velocity space integration, k_θ ($k_\perp$) is the poloidal (perpendicular to $\mathbf{B}$) component of the wave vector $\mathbf{k}$, $\lambda_H = (k_\perp v_\perp)/\omega_{cH} = \sqrt{1+z^2}(|k_\theta|v_\perp)/\omega_{cH}$, $\omega_{cH} = (e_HB/m_Hc)$ is the fast ion cyclotron frequency, $QF_{0H} = (2\omega\partial/\partial v^2 + \mathbf{k}\times\mathbf{b}\cdot\nabla/\omega_{cH})F_{0H}$, $\mathbf{b} = \mathbf{B}/B$, and F_{0H} is the fast ion tail distribution function. The expression of Λ_m including the resonant response of fast ions is given in Eq. (C5) of Appendix C, where some details of its derivations are also discussed.

For $\Omega_{A,m}+\Omega_{A,m-1} \gg r_0/R_0$, the local ($r \simeq r_0$) structure of the shear Alfvén continuous spectrum is shown in Fig. 1. There, it is evident that the typical frequency gap between the local minimum of the $(m-1,n)$ mode continuum and the local maximum of the (m,n) mode continuum is larger than the frequency shift due to toroidal coupling. Thus, toroidal coupling between (m,n) and $(m-1,n)$ modes can be neglected. The two modes, then, satisfy the following approximate dispersion relations, derived from a variational principle:[3]

$$\sqrt{\Omega_{A,m}+\Omega} = \frac{S\pi}{2^{5/2}n^{1/2}}\left(\frac{2n}{S^2}\frac{\Lambda_m}{\Omega_{A,m}}-1\right),$$
$$\sqrt{\Omega_{A,m-1}-\Omega} = \frac{S\pi}{2^{5/2}n^{1/2}}\left(\frac{2n}{S^2}\frac{\Lambda_{m-1}}{\Omega_{A,m-1}}-1\right), \tag{3}$$

where $\Lambda_{m-1}/\Omega \simeq \Lambda_m/\Omega < 0$.

The existence condition of radially localized eigenmodes implies that the left-hand side of Eqs. (3) is real and positive definite. For this reason, Eqs. (3), derived in a similar structure also in Ref. 6, confirm that no GAE can exist in the high-n limit[13,14] in the absence of fast ions ($\Lambda_{m-1},\Lambda_m \to 0$). Furthermore, $\Lambda_{m-1}/\Omega \simeq \Lambda_m/\Omega < 0$ since $\overline{\omega}_{dH} \gg \omega$; thus, in this *very energetic* limit, fast ions are characterized by *negative compressibility*, which causes the mode frequency to be shifted *upward*, contrary to the general case for which fast ion compression shifts the mode frequency downward[1–3] (for a detailed discussion of this point cf. Appendix C). For this reason and because of the local structure of the shear Alfvén continuous spectrum shown in Fig. 1, only the (m,n) mode can exist just above the local maximum of the Alfvén continuum at r_0. On the contrary, the $(m-1,n)$ mode cannot be radially localized at $r \simeq r_0$ with a frequency just below that of the local minimum of the shear Alfvén continuum.

The *frequency localization* of the (m,n) mode just above the local maximum of the Alfvén continuum at r_0 reflects the parametric dependencies of the mode frequency on the local equilibrium parameters. More specifically, a drop in q_0, due to, e.g., current diffusion, induces an increase in the value of the local maximum of the Alfvén continuum. This change would produce an *upwards frequency chirping* of the (m,n) mode on the characteristic time scale of q_0 evolution, as in the case of Alfvén cascades.[6,7] This argument could be clearly made in the opposite sense should the sign of Λ_m change, e.g., because of different characteristic properties of the fast ion dynamics. This issue is analyzed in detail in Appendix C and has important implication on the characteristic variation of the mode frequency when the value of q_0 drops, as observed experimentally.[5–7] In fact, with $\Lambda_m < 0$ *upwards chirping frequencies* are to be expected, as discussed above. On the contrary, for $\Lambda_m > 0$ the $(m-1,n)$ mode would be excited just below the local minimum of the Alfvén continuum at r_0 and *downwards frequency chirping* modes would appear.

The condition for the existence of the (m,n) mode is $\Lambda_m/\Omega_{A,m} > S^2/2n$ [that for the existence of the $(m-1,n)$ mode would be $\Lambda_{m-1}/\Omega_{A,m-1} > S^2/2n$], which is independent on the mode frequency[6] as a consequence of Eq. (2). This condition turns out to be a lower bound on the fast ion tail particle density, n_H, and for the case discussed in Ref. 5 [JET discharge 49382 in the time interval 43.5 s$<t<$44.0 s; $S=1.54$, $-n_H/(R_0\partial_r n_H)=0.13$] it gives $n_H/n_e > 3.1\%$ at $r=r_0$, consistently with the experimental values $(n_H/n_e=4\%)$. Here, n_e is the electron density. Evidently, this criterion of *existence of a gap mode* corresponds to that of vanishing of the local continuum damping (cf. Fig. 1). Note that, by *local* continuum damping, we define the damping associated with the mode interaction with the shear Alfvén continuum at $r=r_0$, where the mode is localized. However, the criterion of *existence of a gap mode* is not sufficient for the mode excitation. In fact, other damping mechanisms are important in the absence of local continuum damping, as *nonlocal continuum damping*, radiative damping[15,16] and ion Landau damping.[17] From Fig. 1, it is clear that nonlocal continuum damping is most important for the (m,n) mode: in fact this damping mechanism would affect the $(m-1,n)$ mode only if toroidal coupling with the (m,n) sideband is considered. Nonetheless, the "selection rule" for the mode excitation would still be that on the sign of Λ_m (i.e., the particle dynamics, as discussed above and in greater detail in Appendix C), because that would determine for which mode the dominant damping mechanism, i.e., local continuum damping, may vanish. Figure 1 also suggests that nonlocal continuum damping should depend on the mode frequency and, more precisely, decrease for increasing Ω. In fact, including this effect, in Appendix A it is demonstrated that the dispersion relation for the (m,n) mode is modified into

$$\sqrt{\Omega_{A,m}+\Omega}\left[1+i\exp\left(-4\sqrt{-n\Omega_{A,m}}/S\right)\right] = \frac{S\pi}{2^{5/2}n^{1/2}}\left(\frac{2n}{S^2}\frac{\Lambda_m}{\Omega_{A,m}}-1\right). \tag{4}$$

From this expression, we note that nonlocal continuum damping is important at low frequency and that it becomes exponentially small for increasing $-\Omega_{A,m}$. This fact provides an explanation of the reason why Alfvén cascades[6] are observed only above a minimum threshold frequency (cf. Fig. 2). From Eq. (4), in fact, we have that the real frequency of the (m,n) EPM gap mode ($\sqrt{\Omega_{A,m}+\Omega_r}$ is real, i.e., vanishing local continuum damping) is given by

$$\sqrt{\Omega_{A,m}+\Omega_r} = \frac{S\pi}{2^{5/2}n^{1/2}}\left(\frac{2n}{S^2}\frac{\mathbb{R}\mathrm{e}\,\Lambda_m}{\Omega_{A,m}}-1\right), \tag{5}$$

while the mode growth rate is obtained from

$$\Gamma = 2\sqrt{\Omega_{A,m}+\Omega_r} \times\left[\frac{\pi n^{1/2}}{2^{3/2}S}\frac{\mathbb{I}\mathrm{m}\,\Lambda_m}{\Omega_{A,m}}-\sqrt{\Omega_{A,m}+\Omega_r}\exp\left(-4\sqrt{-n\Omega_{A,m}}/S\right)\right], \tag{6}$$

where $\Omega\equiv\Omega_r+i\Gamma$. In particular, Eq. (6) gives the excitation condition for the gap mode, i.e., the condition for the mode drive ($\propto -\mathbb{I}\mathrm{m}\,\Lambda_m$, i.e., the resonant fast ion response) to overcome nonlocal continuum damping. As pointed out in Ref. 6, the condition in Eq. (6) is not the usual *resonant* EPM excitation condition, that is normally written without assuming the existence of a gap mode[1–4] ($\sqrt{\Omega_{A,m}+\Omega_r}$ is imaginary and local continuum damping is finite).

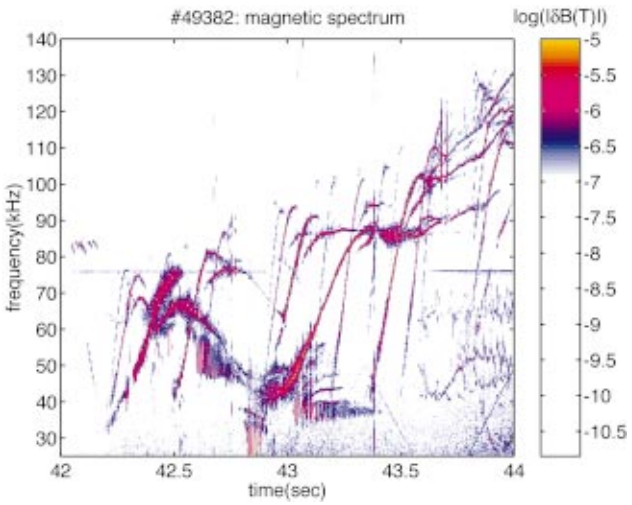

FIG. 2. (Color) Magnetic spectrum in the preheating phase of a JET RS plasma with nonmonotonic q profile (Ref. 5). See also Ref. 6.

For $\mathbb{R}\mathrm{e}\,\Lambda_m>0$, the (m,n) EPM gap mode can no longer be excited. As discussed in Appendix C, the sign of $\mathbb{R}\mathrm{e}\,\Lambda_m$ depends on the details of the fast ion distribution function: in particular on the ratio between the characteristic fast ion thermal speed and the Alfvén velocity. Experimental control on this parameter (the velocity ratio) provides a control on the excitation of either one of the two EPM gap modes, as described by Eqs. (3). Generally, a transition from $\mathbb{R}\mathrm{e}\,\Lambda_m<0$ to $\mathbb{R}\mathrm{e}\,\Lambda_m>0$ results in a transition from the (m,n) EPM to the the $(m-1,n)$ EPM gap mode excitation. However, (m,n) and $(m-1,n)$ EPM gap mode excitations are not mutually exclusive. In fact, Eq. (C5) shows that $\mathbb{R}\mathrm{e}\,\Lambda_m$ depends, among other parameters, both on the velocity ratio and on the mode frequency. Specifically, $\mathbb{R}\mathrm{e}\,\Lambda_m$ is $\propto -\Omega$ and negative for $\Omega\to 0^+$, whereas it is $\propto c_1+c_2/\Omega$ $(c_1,c_2>0)$ for $\Omega\gg 1$. For intermediate values of Ω, $\mathbb{R}\mathrm{e}\,\Lambda_m$ generally has one zero, Ω_0, the value of which depends, e.g., on the velocity ratio. Thus, for $\Omega_0<-\Omega_{A,m}<\Omega_{A,m-1}$ only the $(m-1,n)$ EPM gap mode may exist; for $-\Omega_{A,m}<\Omega_0<\Omega_{A,m-1}$ both $(m-1,n)$ and (m,n) EPM gap modes can be excited; for $-\Omega_{A,m}<\Omega_{A,m-1}<\Omega_0$ only the (m,n) gap mode may exist. As it is also discussed in Appendix C, the present results suggest the interesting possibility of designing experimental operation scenarii for switching from *upwards frequency chirping to downwards frequency chirping* modes by simply controlling the fast ion tail energy, e.g., acting on the density of the minority ion species. Even further, we have actually demonstrated that experimental scenarii are possible where both *upwards and downwards* frequency chirping modes are simultaneously excited at the radial location of a minimum-q surface, with the frequency of the downwards frequency chirping mode being always larger than that of the upwards chirping mode. The strength of the fast ion drive

depends on the details of the particle distribution function and must be determined from Eq. (C5) in each case. Here, we note that the sign of the energetic particle resonant drive ($\propto -\mathbb{I}\mathrm{m}\,\Lambda_m$) is consistent with mode destabilization. In fact $\mathbb{I}\mathrm{m}\,\Lambda_m, \mathbb{I}\mathrm{m}\,\Lambda_{m-1} < 0$, as it may directly verified from Eq. (C5) assuming centrally peaked energetic ion pressure profiles.

The resonant excitation of the $(m-1,n)$ or (m,n) gap modes, as described in Eqs. (3), is not always possible. In fact, gap modes are preferably excited only if the downward or, respectively, upward frequency shift due to the nonresonant response of the fast ions is smaller than the width of the shear Alfvén continuum frequency gap, i.e., $\Omega_{A,m} + \Omega_{A,m-1}$. Thus, the existence of EPM gap modes would depend both on the details of the fast ion dynamics and on the q profile or, more precisely, on the values of q_0 and S. The *transition* from EPM gap modes to resonant EPM excitation can be controlled experimentally in two ways: acting on q_0, e.g., changing the width of the shear Alfvén continuum frequency gap; or varying the additional heating power on fast ions, i.e., controlling the magnitude of frequency shift due to energetic particle compression. As explicitly shown later in this section, a smooth transition from EPM gap mode to resonant EPMs takes place when the fast ion induced frequency shift overcomes the typical width of the shear Alfvén continuum frequency gap.

If no gap mode exists, but still $\mathbb{R}\mathrm{e}\,\Lambda_m < 0$, the (m,n) *resonant* EPM real frequency would be given by

$$\frac{2n}{S^2}\,\frac{\mathbb{R}\mathrm{e}\,\Lambda_m(\Omega_r)}{\Omega_{A,m}} = 1, \tag{7}$$

whereas the EPM growth rate would be obtained from

$$\Gamma = \left(\frac{\partial\,\mathbb{R}\mathrm{e}\,\Lambda_m}{\partial\Omega_r}\right)^{-1}\left(-\mathbb{I}\mathrm{m}\,\Lambda_m + \frac{2^{3/2}S}{\pi n^{1/2}}\Omega_{A,m}\sqrt{-(\Omega_{A,m}+\Omega_r)}\right). \tag{8}$$

For $\mathbb{R}\mathrm{e}\,\Lambda_m > 0$, the analogous dispersion relation for the $(m-1,n)$ mode could be derived similarly, and it can be actually obtained from Eqs. (7) and (8) by simple change of poloidal mode number labels and with the substitution of the real quantity (local continuum damping), $\Omega_{A,m}\sqrt{-(\Omega_{A,m}+\Omega_r)} \Rightarrow -\Omega_{A,m-1}\sqrt{\Omega_r - \Omega_{A,m-1}}$. Equation (8) yields a destabilization condition which obviously requires a stronger particle source than Eq. (6). This fact provides confirmation of the above discussion on which experimental parameters can control the transition between situations characterized by EPM gap modes—described by Eqs. (5) and (6)—to scenarii in which *resonant* EPMs—described by Eqs. (7) and (8)—can be excited. The obvious sensitive parameter is the level of power input, although adjusting the localization of power deposition (power density) would serve to the same scope by changing the local gradient in the fast ion energy density.

As $\Omega_{A,m} + \Omega_{A,m-1} \to 0^+$ (which may occur when q_0 drops, as in the experiment), toroidal coupling effects become more important (cf. Fig. 3). Following the theoretical approach of Ref. 3 (details are given in Appendix B), the modified EPM dispersion relation in the toroidal case is derived in the form

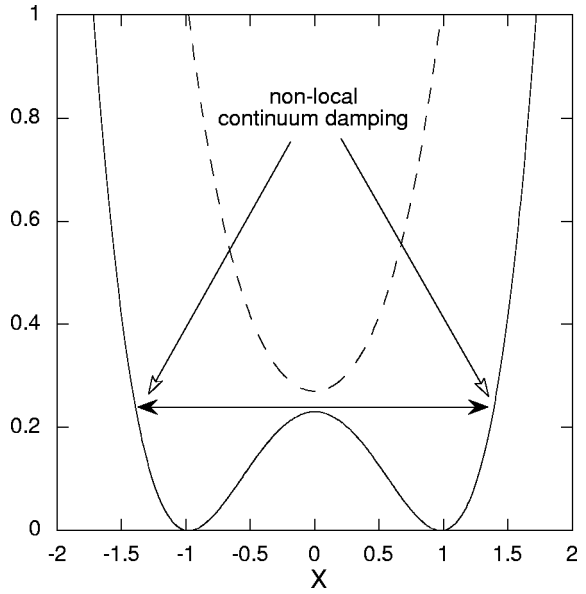

FIG. 3. Radial structure of the shear Alfvén continuous spectrum for the (m,n) and $(m-1,n)$ modes in the case $\Omega_{A,m} + \Omega_{A,m-1} \approx r_0/R_0$. The value of $q^2 R_0^2 k_{\|m,n}^2$ is shown vs $x \equiv \sqrt{nq_0''}(r - r_0)$. The frequencies of the *even* parity toroidal mode is also shown as expected from Eq. (9).

$$\begin{aligned}
&[\epsilon_0^2\Omega^4 - (\Omega^2 - 1/4)^2]^{1/4} \\
&\quad = -\frac{S\pi}{4n^{1/2}}\left[\left(1 \pm 4\frac{n\Lambda_m}{S^2}\right)\right. \\
&\qquad \left. + \mathrm{sgn}(\cdot)\sqrt{\left(1 \pm 4\frac{n\Lambda_m}{S^2}\right)^2 + \frac{16\epsilon_0 n}{\pi^2 S^2}}\right], \\
&\mathrm{sgn}(\cdot) = \mathrm{sgn}\,\mathbb{R}\mathrm{e}\left(1 \pm 4\frac{n\Lambda_m}{S^2}\right),
\end{aligned} \tag{9}$$

where $\epsilon_0 \equiv 2(r_0/R_0 + \Delta')$, $\Omega_{A,m} \simeq -1/2$ and Δ' denotes the derivative of the Shafranov shift. Furthermore, the upper (lower) sign refers to modes excited near the lower (upper) accumulation point of the shear Alfvén continuous spectrum. Of the two modes described by Eq. (9), one is an EPM gap mode, while the other is strongly continuum damped (cf. Appendix B for details). As in the case of Eqs. (3), the selection rule between the two modes is given by the sign of $\mathbb{R}\mathrm{e}\,\Lambda_m$: $\mathbb{R}\mathrm{e}\,\Lambda_m < 0$ upper sign, $\mathbb{R}\mathrm{e}\,\Lambda_m > 0$ lower sign. Note also that the fourth root of the quantity in parentheses appears on the left-hand side of Eq. (9), due to the local minimum in the q profile, and not the square root as in the usual TAE case with $q_0' \neq 0$.[3,10]

Equation (9) gives the most unstable EPM root near the excitation threshold. However, as discussed in Appendix B, given an EPM gap mode effectively excited at $\Omega^2 \simeq (1/4) \times (1 \pm \epsilon_0)$, a much more weakly driven gap mode exists also near $\Omega^2 \simeq (1/4)(1 \mp \epsilon_0)$, and its frequency is given by

$$[\epsilon_0^2\Omega^4-(\Omega^2-1/4)^2]^{1/4}$$
$$=-\frac{S\pi}{4n^{1/2}}\left[\left(1\pm 4\frac{n\Lambda_m}{S^2}\right)\right.$$
$$\left.-\mathrm{sgn}(\cdot)\sqrt{\left(1\pm 4\frac{n\Lambda_m}{S^2}\right)^2+\frac{16\epsilon_0 n}{\pi^2 S^2}}\right]. \quad (10)$$

This increased multiplicity of roots is due to the effect of toroidicity only, and can be considered a consequence of the existence, at $r=r_0$, of four nearly degenerate shear Alfvén waves at the frequency of the toroidal gap in the Alfvén continuous spectrum. The complete toroidal EPM dispersion relation is actually given by Eq. (B5), that recovers both Eqs. (9) and (10) near threshold in the toroidal case, and Eqs. (3) for negligible toroidal coupling. Clearly, the *exponentially small* continuum damping, due to the nonlocal interaction with the mode continuum, and other kinetic damping mechanisms, e.g., radiative damping[15,16] and ion Landau damping,[17] must be evaluated and compared with the resonant drive associated with fast ions,[3] as obtained from Eq. (C5), before the existence of such modes is demonstrated on a rigorous basis. From the results of Eq. (4) on the magnitude of nonlocal continuum damping, we may however conclude that the most important damping mechanism for the toroidal EPM gap mode is radiative damping or ion Landau damping, which are neglected in the present analysis for the sake of simplicity.

Equation (9) gives a unified description of the toroidal branches of both EPM gap modes and resonant EPMs in the same way it was discussed in detail for Eq. (3) and what followed. In particular, Eq. (9) shows that, for

$$\left|\left(1\pm 4\frac{n\Lambda_m}{S^2}\right)\right|\gtrsim\sqrt{\frac{16\epsilon_0 n}{\pi^2 S^2}}, \quad (11)$$

a smooth transition is expected from EPM gap modes to resonant EPMs. Equation (11) is the quantitative formulation of the qualitative criterion discussed above for the transition from EPM gap mode to resonant EPMs when the fast ion induced frequency shift overcomes the typical width of the shear Alfvén continuum frequency gap.

When $\Omega_{A,m}+\Omega_{A,m-1}\ll -r_0/R_0$, due, e.g., to a further drop in q_0, the radial structure of the shear Alfvén continuous spectrum becomes that of Fig. 4. The EPM *gap mode* smoothly changes from a radial structure localized near $x=0$ and will eventually end up into a double-hump structure, as it could be quantitatively inferred from transforming back the Fourier mode structures $\delta\phi_m, \delta\phi_{m-1}$ of Eqs. (B2) and (B3) into the corresponding real space eigenfunctions $\delta\psi_m, \delta\psi_{m-1}$.[18] This calculation is tedious but straightforward[18] and it will be omitted here. In any event the double-hump structure of the EPM is fairly reasonable and intuitive from Fig. 4. The radial structure in this case has a *natural* radial width $\approx r_0/(n^{1/2}Sq_0)$, so its effect on transport may be significant. The analysis of the effect on transport due to global mode structures of high-n modes (generally speaking *drift* or *drift-Alfvén* modes) near a minimum-q surface is beyond the scope of the present analysis and will be subject of a future work. Here, we just emphasize that the presence of a weaker source (drive), due to radial redistribution of fast ions, may explain why, after reaching the TAE frequency as in Figs. 3 and 4, the experimentally observed modes disappear[6] (cf. Fig. 2). Another possible explanation is based on Eq. (11). Assuming weak modifications of the fast ion source, the fast ion induced frequency shift is also nearly constant. Meanwhile, the typical gap width in the shear Alfvén continuum decreases as $\Omega_{A,m}+\Omega_{A,m-1}\to 0$, and the criterion of Eq. (11) could be violated. In other words, the fast ion compression effect could be too strong for a toroidal EPM gap mode to exist, and too weak for the excitation of a toroidal resonant EPM. Alfvén cascades, then, may start as weakly driven EPM gap modes at low frequency, described by Eq. (4), and end up in damped toroidal resonant EPMs, described by Eq. (9) (upper sign), as $\Omega\to 1/2$. Both phenomena are always present, but which is the dominant one needs to be determined case by case. Not surprisingly, the response depends crucially on the strength of the fast ion drive and on the details of the energetic particle dynamics. This picture is supported by recent numerical simulations of fast ion transports due to resonantly excited EPMs in hollow q-profile tokamak equilibria,[19,20] that are briefly discussed in Sec. IV. The important fact to appreciate, here, is that the detailed properties of toroidal modes are crucially dependent on fast ion dynamics. In fact, toroidal eigenmodes (i.e., TAEs) can exist at a minimum-q surface even in the absence of fast ions. However, such modes can exist only at very low levels of the thermal plasma pressure and the effect of thermal plasma compressibility is easily exceeded by that of energetic ions (cf. Appendix B), as it happens in the small but finite magnetic shear case.[3] Thus, in the presence of fast ions, the properties of toroidal Alfvén modes are essentially those of toroidal EPMs, discussed above.

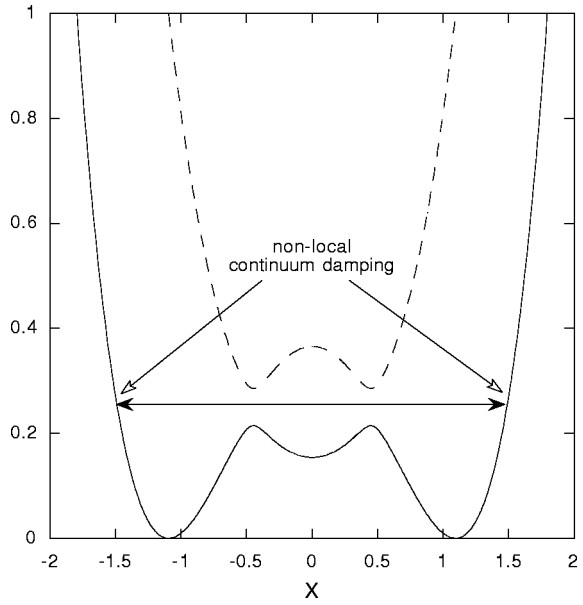

FIG. 4. Radial structure of the shear Alfvén continuous spectrum for the (m,n) and $(m-1,n)$ modes for $\Omega_{A,m}+\Omega_{A,m-1}\ll -r_0/R_0$. The value of $q^2R_0^2k_{\parallel m,n}^2$ is shown vs $x\equiv\sqrt{nq_0''}(r-r_0)$. The frequencies of the *even* parity *double* EPM (toroidal mode) is also shown where it could be expected.

III. EPM EXCITATION AT DIFFERENT RADIAL LOCATIONS: THE LINEAR STABILITY POINT OF VIEW

Here, we address the issue of EPM stability in tokamaks with hollow q profiles looking closely at the stability properties of EPM as we move away from the minimum-q surface. In fact, EPM stability analyses at the minimum-q surface (cf. Sec. II) and those that assume *small but finite shear*[3] appear weakly related, despite the fact that they are all focused on the same problem. In this section, we demonstrate that all these results are actually *consistent* and that they may be presented within a unified picture. For the sake of clarity, we will discuss the problem in the case when toroidal mode coupling can be consistently neglected. The toroidal problem can be analyzed exactly in the same fashion, but with greater technical complexity.

It is part of the common wisdom to assume that, within the usual *ballooning formalism*,[21] the *translational invariance* of radial mode structures breaks down for different poloidal Fourier modes when magnetic shear vanishes. This is evidently true. However, as it was shown in Refs. 18 and 22, only the separation of spatial scales between equilibrium quantities and wavelengths is really needed for the analysis of high-n mode structures. This separation of scales is still valid for high-n modes both near and at a minimum-q surface, where magnetic shear vanishes by definition. This fairly general assumption is the only one made in the following treatment.

The strength of the formalism employing the separation of scales is based on the fact that the fast radial scale and the spatial coordinate along the magnetic field can be considered *Fourier conjugate* variables. This is obvious from the following identities:

$$qR_0k_{\parallel;m,n}=nq_0'(r-r_0)\Rightarrow \mathrm{i}s\frac{\partial}{\partial\kappa_r},\quad q_0'\neq 0, \tag{12}$$

$$qR_0k_{\parallel;m,n}=qR_0k_{\parallel;m,n}(r_0)+\frac{nq_0''}{2}(r-r_0)^2$$

$$\Rightarrow\Omega_{A,m}-\frac{S^2}{2n}\frac{\partial^2}{\partial\kappa_r^2},\quad q_0'=0, \tag{13}$$

where $\kappa_r\equiv(r_0/m)k_r$ and $\delta\phi_m$, the Fourier transform of $\delta\psi_m$, is given by

$$\delta\phi_m(\kappa_r)\equiv\frac{1}{\sqrt{2\pi}}\int_{-\infty}^{\infty}\exp i\left(\frac{m}{r_0}\kappa_r(r-r_0)\right)$$

$$\times\delta\psi_m(r)d\frac{m}{r_0}(r-r_0).$$

Moreover, we have that, respectively, $s\equiv r_0q_0'/q_0$ and $S\equiv\sqrt{r_0^2q_0''/q_0^2}$ are the *usual* and *generalized* shear values. Note that for $q_0''<0$ the definition of S would change accordingly and that Eq. (12) assumes $\Omega_{A,m}\equiv qR_0k_{\parallel;m,n}(r_0)=0$, as it is always possible for $s\neq 0$. From Eqs. (12) and (13), it is readily shown that

$$q^2R_0^2k_{\parallel;m,n}^2=\Omega_{A,m}^2-\Theta_m\frac{\partial^2}{\partial\kappa_r^2}, \tag{14}$$

where $\Theta_m=s^2$ and $\Omega_{A,m}=0$ for $s\neq 0$, and $\Theta_m=S^2\Omega_{A,m}/n$ for $s=0$. Then, Eq. (1) in Fourier space can be rewritten as

$$\left[\frac{\partial^2}{\partial\kappa_r^2}+\frac{\Omega^2-\Omega_{A,m}^2}{\Theta_m}-\frac{1}{(1+\kappa_r^2)^2}+\frac{\Lambda_m/\Theta_m}{(1+\kappa_r^2)}\right](\sqrt{1+\kappa_r^2}\delta\phi_m)$$

$$=0. \tag{15}$$

This equation is readily obtained from Eq. (A2), which is a reformulation of Eq. (1). We also note that Eq. (15) is exactly Eq. (13) of Ref. 3, where it was derived for the small but finite shear case. A one to one correspondence between these two equations is obtained by noticing that $\Lambda_m\Leftrightarrow\overline{\alpha}_E/4$, where $\overline{\alpha}_E$ is the notation of Ref. 3 for the flux surface averaged contribution of fast ions. More precisely, the expression for $\overline{\alpha}_E$, used in Ref. 3, included the effect of fast ion precessional resonance only and it was written for a single pitch angle distribution function. On the contrary, the expression of Λ_m used here, Eq. (C5) of Appendix C, is written for a general fast ion distribution function and arbitrary precession and precession-bounce resonances. From Eq. (15), we readily obtain the mode dispersion relation in the form

$$\sqrt{-\frac{\Omega^2-\Omega_{A,m}^2}{\Theta_m}}=\frac{\pi}{4}\left(\frac{2\Lambda_m}{\Theta_m}-1\right), \tag{16}$$

which recovers both Eqs. (3) and their analogue for the small but finite shear case discussed in Ref. 3, i.e.,

$$\mathrm{i}\Omega=\frac{|s|\pi}{4}\left(1-\frac{2\Lambda_m}{s^2}\right). \tag{17}$$

The factor Θ_m reflects the typical radial width of the mode structure, Δr. In fact,

$$\left|\frac{m}{r_0}\Delta r\right|^2\approx\left|\frac{\Omega^2-\Omega_{A,m}^2}{\Theta_m}\right|.$$

It is, then, obvious that the largest value of Θ_m between s^2 and $|S^2\Omega_{A,m}/n|$ determines the radial mode width and the actual form of the mode dispersion relation in Eq. (16). Since we may estimate $(\Delta r/r_0)^2\propto|1/m^2\Theta_m|$, the transition from small but finite shear to zero shear, i.e., from Eqs. (3) to (17), occurs for $s^2\lesssim S^2/n$. In general, Eq. (16) could be used to study EPM stability properties at different radial locations, including at the transition from the weak to the zero shear regions. A similar argument could be made for the toroidal extension of Eq. (16), i.e., Eq. (B5) or, more generally, Eq. (B8), that can be used for weak as well as zero magnetic shear and are in a one-to-one correspondence with the toroidal dispersion relation discussed in Ref. 3 as toroidal extension of Eq. (17).

Typical profiles of safety factor q and of fast ion normalized energy density β_H (the normalization being with respect to the magnetic energy density) in JET RS discharges are given in Fig. 5.[5] Note that the q profile in Fig. 5 is derived including motional Stark effect constraints, and that the β_H profile is obtained using the method discussed in Refs. 23 and 24. Figure 6, meanwhile, shows the corresponding profiles for magnetic shear, $s=(r/q)(dq/dr)$, and $\alpha_H\equiv-R_0q^2(d\beta_H/dr)$, which gives an indication of the strength of the fast ion drive. These profiles are a reasonable

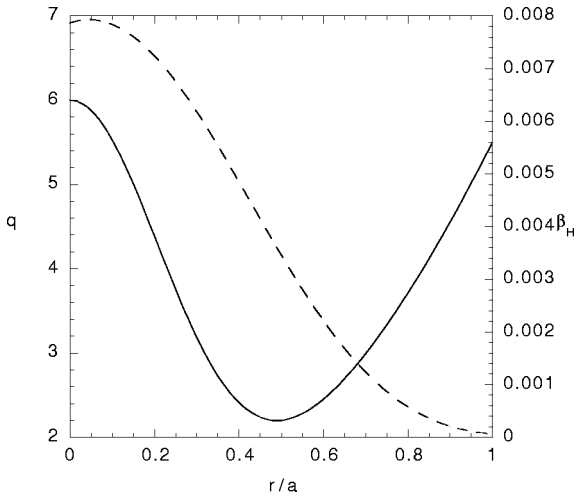

FIG. 5. Radial profile for q (solid line) and β_H (broken line).

model of JET discharge 49382 at a fixed time in the interval 43.5 s$<t<$44.0 s (Ref. 5) and generally represent a good paradigm case to investigate with Eq. (16). Such studies, however, are beyond the scope of the present investigation and, thus, they will be presented in a separate work together with analyses of the toroidal equivalent of Eq. (16), i.e., Eq. (B5). Nonetheless, we wish to emphasize how Fig. 6 suggests that a strong resonant excitation of EPMs should occur at $r/a \approx 0.2$, where α_H is maximum. Indeed, direct numerical 1D–GKE linear simulations[2] confirm this expectation for the present parameters, i.e., at $r/a=0.2$, $s=rq'/q=-0.58$, $q=4.4$, $\alpha=-R_0q^2(d\beta/dr)=0.44$, $\Delta'=0.125$, $\alpha_H=0.515$, $\beta_H=0.0072$, $\eta_H=0.395$, $v_{TH}/v_A=0.43$, $\rho_{LH}/a=0.019$, where β is the thermal plasma normalized energy density, Δ' is the derivative of the Shafranov shift, $\eta_H=\partial_r \ln T_H/\partial_r \ln n_H$ with n_H (T_H) the fast ion density (temperature), $v_{TH}=\sqrt{T_H/m_H}$ is the fast ion thermal speed and v_A is the Alfvén velocity. The simulations assume that the fast ion tail distribution function is a Maxwellian in energy, with a pitch angle distribution highly peaked around $\mu B_0/(v^2/2)=1$, μ being the magnetic moment and B_0 the vacuum magnetic field on axis. Results are shown in Fig. 7, where the growth rate (solid line) and the mode frequency (broken line) of the EPM, normalized to the local Alfvén frequency (v_A/qR_0), are shown vs the fast ion Larmor radius normalized to the inverse poloidal wave number ($k_\theta \rho_{LH}$, lower horizontal scale) or, equivalently, vs the toroidal mode number (upper horizontal scale). The two horizontal dashed lines indicate the local width of the toroidal frequency gap in the Alfvén continuum. The reason why the mode can be considered a resonantly excited EPM and not a toroidal Alfvén eigenmode (TAE)[10] is given by the strength of the growth rate, which generally exceeds the gap between the mode frequency and the continuum accumulation point. A more articulated explanation of this interpretation is provided in Ref. 2.

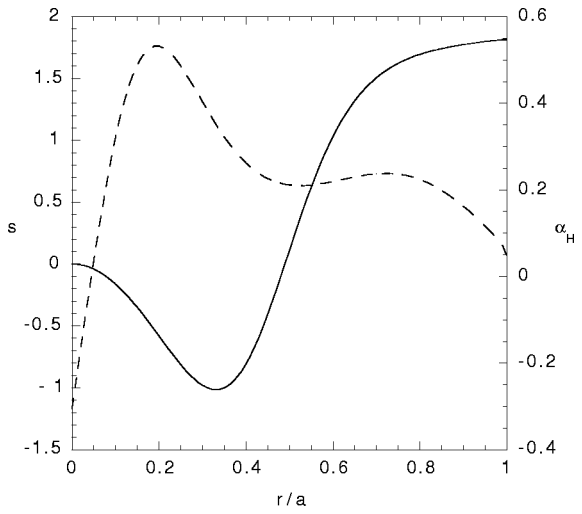

FIG. 6. Radial profile for $s=rq'/q$ (solid line) and α_H (broken line).

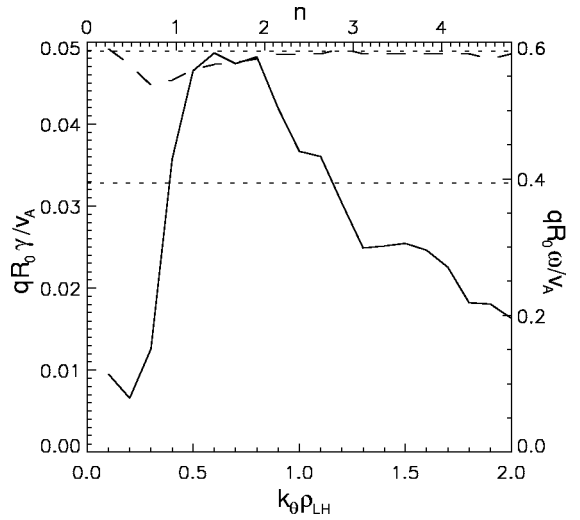

FIG. 7. Local values of growth rate (solid line) and real frequency (broken line) of an EPM at $r/a=0.2$. The two horizontal lines indicate the toroidal gap in the Alfvén continuum (Ref. 5).

On the basis of linear stability analyses, presented so far in Secs. II and III, we may conclude that EPMs are generally excited at different radial locations as either EPM gap modes or resonant EPMs. These modes are described by the same dispersion relation with different dominant damping mechanisms and a smooth transition from one to the other mode can be obtained, e.g., by varying α_H (Refs. 3, 4, 12, and 25) or v_{TH}/v_A.[3] Due to the peculiar role of wave-particle interactions in the mode excitation, resonant EPMs are preferentially excited *within* the minimum-q surface, where the mode drive is expected to be strongest. Other Alfvénic modes are usually not excited in the plasma core region inside the minimum-q surface due to finite-α stabilization of TAE modes via strong continuum damping.[3,4,22,26–28] The threshold condition for finite-α TAE stabilization is very low for low magnetic shear, $\alpha>\alpha_{\rm crit}=r_0/R_0+2\Delta'+s^2$,[29–31] and it can be easily exceeded.[3] Thus, if the excitation condition of resonant EPMs is not satisfied in the plasma core, TAE modes can be generally expected only in strongly reversed q profiles, around the most negative shear position, where $\alpha_{\rm crit}$ is maximum and the condition $\alpha<\alpha_{\rm crit}$ is more likely to occur.[4,22] EPM gap modes, meanwhile, are affected by weaker damping mechanisms and are preferentially excited

at the minimum-q surface for two basic reasons: (i) this is the place where a frequency gap *naturally* appears in the shear Alfvén continuous spectrum even for negligible toroidal coupling;[6] (ii) this is also the innermost surface where the downwards frequency shift due to thermal plasma compression (finite α) is relatively small and, at the same time, the strength of the mode drive is relatively large.

The radial localization, growth rate, and mode structure of the most unstable EPM are determined mainly by fast ion pressure and q profiles. Thus, on basis of previous discussions, a great variety of scenarii is possible and case by case must be considered for detailed discussion. Nonetheless, we may draw some general conclusions when looking at the different qualitative behaviors we could expect. To do so, we assume reasonable profiles as those of Figs. 5 and 6, and take β_{H0}, the value of β_H on axis, as *control* parameter to move from one regime to another.

Starting from low β_{H0}, the first EPM to be excited is the EPM gap mode at the minimum-q surface. Call this first threshold value $\beta_{H0,\ell}$. Meanwhile, the q profile of Fig. 5, can be considered as strongly reversed since $s=-0.58$ at the position of maximum α_H and $s\lesssim -1$ at $r/a\simeq 0.3$. In fact, in the absence of fast ions and consistently with what is expected from the discussion above, the local TAE dispersion relation[22] predicts the existence of a toroidal gap mode with $\Omega=0.53$ at $r/a=0.2$, for the core plasma parameters used in the simulation in Fig. 7. Furthermore, radial positions of most negative shear (maximum α_{crit}) and maximum α_H are nearly the same. For this reason, the toroidal gap mode at $0.2\lesssim(r/a)\lesssim 0.3$ is characterized by both strong drive as well as weak damping. Thus, for $\beta_{H0}\gtrsim\beta_{H0,\ell}$ we conclude that two EPM gap modes should be excited, one at the minimum-q surface and another at the radial position which gives the best compromise between maximizing α_H and minimizing s (i.e., maximizing α_{crit} for finite α enhanced continuum damping).

Increasing β_{H0} further, we reach a second threshold value, $\beta_{H0,u}$, above which the mode inside the minimum-q surface is excited as resonant EPM. Strong resonant excitation of such instability generally yields rapid particle transport and frequency chirping on time scales that are shorter than any characteristic time of equilibrium changes.[3] Due to its resonant character, the mode is preferentially excited at the position of maximum drive, which is typically that of maximum α_H. However, this is not always the case, since orbit averaging effects, which are sensitive to the q profile, may play an important role. Changing the profiles from those of Figs. 5 and 6 allows us, in principle, to have situations in which, for $\beta_{H0}\gtrsim\beta_{H0,u}$, we could have a transition of the EPM gap mode at the minimum-q surface into a resonant EPM before the excitation of resonant EPMs inside the minimum-q surface.

The actual values of $\beta_{H0,\ell}$ and $\beta_{H0,u}$ depend both on the profiles and on the relevant wave-particle resonance. For example, these values would be different for transit resonances with circulating ions and for precession-bounce resonances with trapped particles, as in the case of ICRH. Nonetheless, the qualitative plot of possible excitation scenarii, discussed above, remains the same, regardless to the details of wave-particle dynamics. Linear theory, presented in Secs. II and III, indicates that $\beta_{H0}\gtrsim\beta_{H0,u}>\beta_{H0,\ell}$ for the profiles of Figs. 5 and 6.

From the experimental point of view, resonant EPMs excited deep in the plasma core have a high poloidal mode number due to the high local value of q: thus, they would be difficult to be detected by MHD loops located at the plasma edge. Their direct detection would require adequate diagnostics for spatially resolved fluctuation measurements, as reflectometry, which already proved to be successful in measuring core localized Alfvénic activity.[32,33] However, there could be severe requests on the time resolution that is actually required for detecting fast frequency chirping that is expected for strong resonant EPM excitation.[3] As it is demonstrated in the next section, the chirping rate scales naturally as the inverse mode growth rate. Measuring the ''asymptotic'' frequency of the nonlinearly saturated resonant EPMs is an easier task since it involves resolving the characteristic lifetime of the nonlinear structures. Direct measurement of EPM gap modes is much less cumbersome, since these modes are radially localized at the position of the minimum-q surface and are typically characterized by smaller poloidal mode numbers than those of the resonant EPMs excited in the plasma core. Magnetic fluctuation measurements at the plasma edge are the readily available diagnostic in this respect, as it is remarkably shown by observations of Alfvén cascades,[6–9] that have largely motivated the present theoretical investigation.

Fluctuation measurements obviously provide direct proof of the type of modes that are excited in actual experimental conditions. An indirect but nonetheless very interesting option to provide evidence of resonant EPM excitation, is given by measuring the actual fast ion distribution, both in space (radial) and energy. The discussion of such aspect takes us into a truly nonlinear dynamical picture, which is the topic of the next section.

IV. EPM EXCITATION AT DIFFERENT RADIAL LOCATIONS: THE NONLINEAR DYNAMIC POINT OF VIEW

In the present section, we discuss the broader framework of EPM stability and EPM induced transport in tokamaks with hollow q profiles. From the discussions presented in Sec. III, we concluded that both resonant EPMs inside the minimum-q surface and EPM gap modes are excited for the profiles of Figs. 5 and 6. The former short wavelength modes are excited deep in the plasma core and are difficult to be detected by MHD loops located at the plasma edge. The latter fit well with experimental evidence of Alfvén cascades,[6–9] as remarkably demonstrated by magnetic fluctuation measurements.

In the presence of two linearly unstable modes, excited at different radial locations, two qualitatively different and limiting scenarii are possible for the nonlinear mode evolution. In the first moderate-drive scenario, the fast particle transport time scale between regions where different modes are excited is long compared with the inverse mode growth rates. Then, both modes evolve nonlinearly in an indepen-

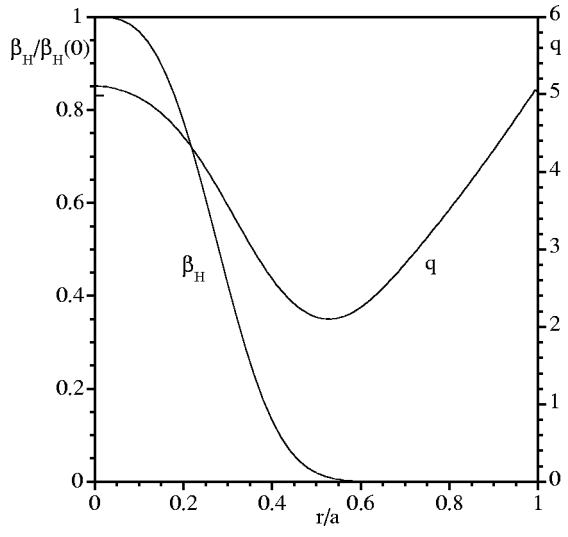

FIG. 8. Radial profiles of q and β_H that are used in the nonlinear simulations with the HMGC code (Refs. 11 and 12).

dent fashion and can be considered separately. In the second strong-drive scenario, the inner mode grows and induces nonlinear fast particle redistributions (transport) on a characteristic time which is shorter or comparable with the inverse growth rate of the outer mode. In this case, the problem is intrinsically nonlinear and modes excited at different radial locations cannot be considered independently. For the sake of precision, we may not exclude that the outer mode could be the most rapidly growing. This situation, however, is not typical, as it is discussed in detail at the end of Sec. III and we will not further comment on that.

The two limiting scenarii discussed above are qualitatively illustrated in the following nonlinear numerical studies using a Hybrid MHD-Gyrokinetic Code (HMGC).[11,12] The q and β_H profiles used in the simulations are those of Fig. 8, an isotropic Maxwellian is assumed for the fast ion distribution function, and $\rho_{LH}=0.01$, $v_{TH}/v_A=1$ are kept fixed. For $\beta_{H0}=0.008$, we are in the first moderate-drive scenario and, relative to the discussion at the end of Sec. III, we have $\beta_{H0}\gtrsim\beta_{H0,u}>\beta_{H0,\ell}$. Simulations show that, after a transient phase, a resonant EPM is excited at the radial position of maximum drive. Results are shown in Fig. 9. After saturation, without significant radial redistribution of the fast ion source, the resonant EPM reaches a time asymptotic fluctuation amplitude at a comparable level with that of a more weakly growing EPM gap mode, which appears at later times, as shown in Fig. 10. Discussing the details of nonlinear dynamic evolution and saturation processes is beyond the scope of the present paper. These and other results are analyzed elsewhere.[34]

At $\beta_{H0}=0.022$, well above the resonant EPM excitation threshold, we are in the second strong-drive scenario and $\beta_{H0}>\beta_{H0,u}>\beta_{H0,\ell}$. Nonlinear simulations[19,20] demonstrate that, in such conditions, very rapid radial redistributions of fast ions take place on a time scale that is proportional to the inverse EPM growth rate (typically $\approx 100\tau_A$, $\tau_A=R_0/v_A$ being the Alfvén time). In the linear destabilization phase, Fig. 11 evidentiates strong resonant excitations of EPM around the position where the resonant drive is strongest, i.e., at $r/a\approx 0.3$. As a demonstration of the resonant character of the mode, the mode structure evolves as the fast ion source is radially displaced and weakened, till the mode merges into a weakly driven Alfvén mode near the frequency gap at the radial position of the q-minimum surface, $r/a\approx 0.5$ (cf. Fig. 12). This rapid nonlinear evolution suggests that, in the case of strong resonant EPM excitation inside the minimum-q surface, these modes would basically serve as strong scattering mechanism for the fast ions and quickly disappear after the particle radial redistribution. The case at $\beta_{H0}=0.022$, with strongly driven resonant EPMs, clearly shows that there can be a strong connection between modes excited at different radial locations. In this case, EPM excitation near the minimum-q surface is an intrinsically non-linear process that should be analyzed together with particle transport.

From a comparison of the contour plots of Figs. 10 and 12, no major differences emerge in the asymptotic states of the EPM gap mode frequency spectra. Meanwhile, fundamental differences clearly emerge by direct comparison of asymptotic fast ion radial profiles. For low β_{H0}, radial fast particle transport does not significantly affect the initial radial distribution: resonant EPM and EPM gap mode, excited at different radial locations, can be assumed as linearly unstable modes that independently evolve on different characteristic time scales and eventually saturate via *independent* nonlinear dynamic evolutions. On the contrary, for $\beta_{H0}=0.022$, strong and fast radial particle transport significantly affects the linear destabilization of the EPM gap mode. If it were not for such fundamental differences in the fast ion dynamics, from experimental measurements of magnetic fluctuation frequency spectra one could hardly draw conclusions on any significant difference for these two scenarii. The long time scale behavior of the mode frequency would, in both cases, follow the adiabatic changes in the local equilibrium quantities. For the *very energetic fast ion tail* limit, discussed in Sec. II, the trend would be that of *upwards frequency chirping*, as observed for *Alfvén cascades*.[6–9]

The complexity and richness of nonlinear fast ion dynamic behavior and of self-consistent description of EPM excitations emerges clearly from the present analysis. This fact should always be considered in discussions of experimental results since very different energetic particle transports may take place despite the very similar Alfvénic character of observed modes. Therefore, actual measurements of fast ion distribution functions (both in space and energy) and of radially resolved frequency spectra are simultaneously needed to draw conclusions and to make any significant comparison between theory and experiment. In the absence of spatially resolved fluctuation measurements, knowledge of fast ion distribution functions could nonetheless be useful and provide indirect but still important information about the modes that are actually excited in realistic experimental conditions. If measured energetic particle profiles were significantly different from those expected on the basis of power density deposition, our analysis would suggest strong resonant EPM excitation inside the minimum-q surface as a good candidate to explain such a discrepancy.[34] No useful information would be provided in the opposite case.

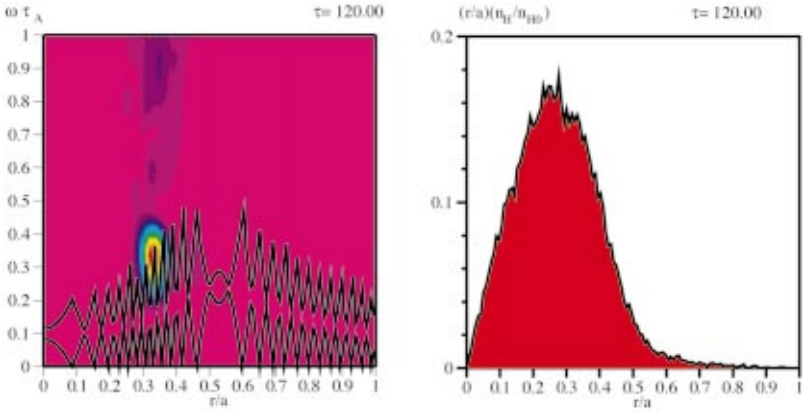

FIG. 9. (Color) Contour plot (left) of the EPM scalar potential fluctuation intensity in the $(r/a,\omega\tau_A)$ plane at $\tau=t/\tau_A=120$, in the linear destabilization phase. Here, $\beta_{H0}=0.008$ and $\tau_A=R_0/v_A$ is the Alfvén time. The shear Alfvén continuous spectrum is also shown for reference in the background. The initial fast ion radial distribution (right), $(r/a)(n_H/n_{H0})$, is also shown as a function of r/a.

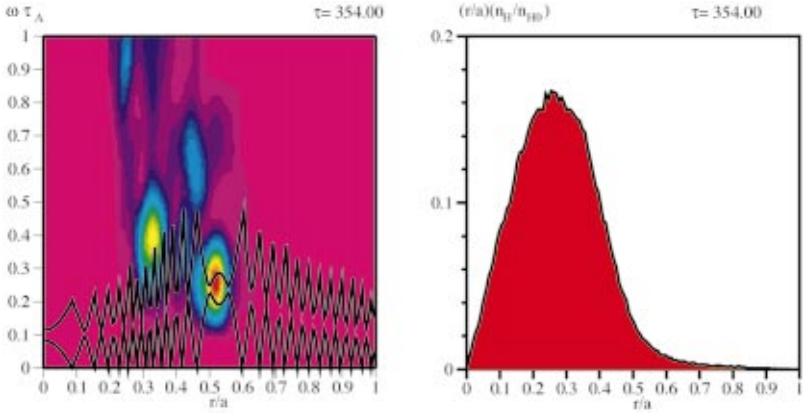

FIG. 10. (Color) Same as Fig. 9, but at $t=354\tau_A$, in the fully nonlinear saturated phase. The fast ion radial distribution (right), $(r/a)(n_H/n_{H0})$, does not indicate significant modifications from that of the initial state.

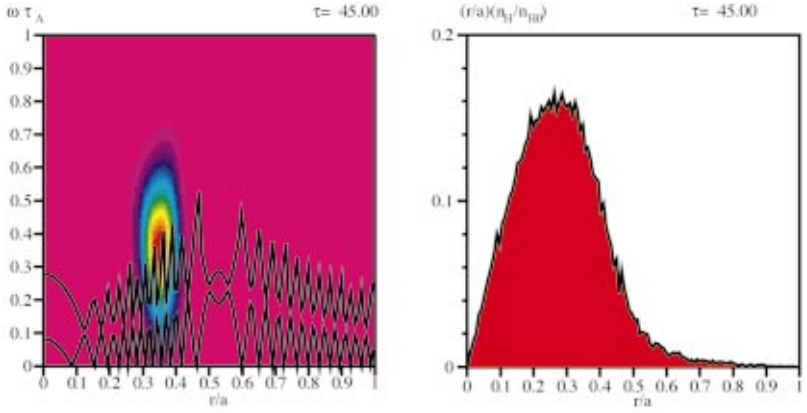

FIG. 11. (Color) Same as Fig. 9, but with a stronger drive. Here, $\beta_{H0}=0.022$ and $t=45\tau_A$, in the linear destabilization phase.

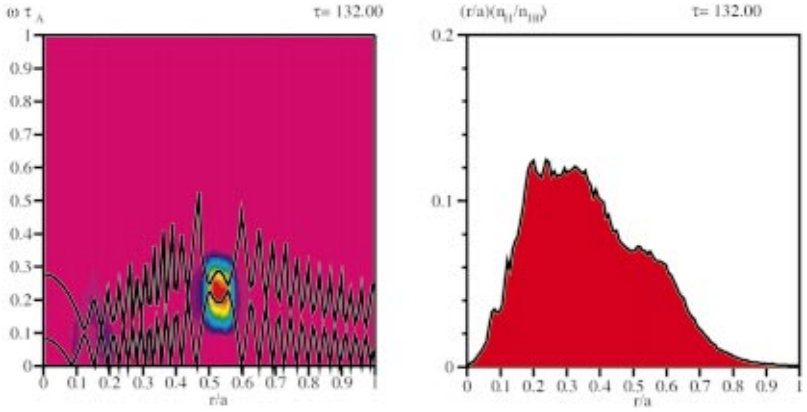

FIG. 12. (Color) Same as Fig. 11, but at $t=132\tau_A$, in the fully nonlinear saturated phase. The fast ion radial distribution (right), $(r/a)(n_H/n_{H0})$, shows strong modifications when compared with that of the initial state, confirming significant and rapid radial particle transport.

The question of resonant EPM excitation within the minimum-q surface and of the rapid fast ion radial transport that such modes may cause has been recently analyzed.[19,20,34] More careful comparisons with experimental observations require detailed analyses that will be presented elsewhere, since they are beyond the scope of the present work. Here, as a final remark, we note once more that resonant EPMs, if at all excited, would yield rapid particle transports on a time scale that, for most present tokamaks, would be of ≈ 1 ms. Such rapid transport events have been recently observed in JT-60U during N–NBI (negative neutral beam injection) and have been named abrupt large amplitude events, ALE.[35]

V. DISCUSSION AND CONCLUSIONS

In this work, we have presented a thorough analysis of EPM stability and mode structures in tokamaks with hollow q profiles. From the point of view of EPM excitations by ICRH fast ion tails, we have shown the importance of both the region inside the minimum-q surface and of the toroidal annulus of width $s^2 \lesssim S^2/n$, centered at r_0.

In the region near the minimum-q surface, we have shown that two types of EPMs may exist. The first type are EPM gap modes, for which the existence condition as localized modes with frequency inside the gap in the shear Alfvén continuous spectrum is equivalent to the condition of vanishing local continuum damping. For such modes, the dominant damping mechanism is nonlocal continuum damping. The second type of EPMs are resonant EPMs, with real frequency given by Eq. (7) and determined essentially by fast ion compressibility effects, and with growth rate set by the competition of resonant drive and local continuum damping, as in Eq. (8). Generally speaking, however, the distinction between the two types of EPMs appears somewhat artificial since they are given by the same dispersion relation and a smooth transition from one type to the other may be obtained by controlling the fast ion distribution function or, equivalently, their fundamental dynamic properties. When toroidal coupling becomes important and nonlocal continuum damping is exponentially small, due to the higher mode frequency, the dominant damping mechanism for EPM gap modes is radiative damping or ion Landau damping, that are not included in the present analysis for the sake of simplicity. Besides this aspect, the ''distinction'' between the two types of EPMs remains as discussed above. Meanwhile, it is demonstrated that EPMs with frequency near the TAE gap may have either single or double hump radial structures.

A detailed discussion of the fast ion resonant and nonresonant response is also presented in connection with its crucial importance in determining the characteristic signatures of the excited EPMs, e.g., the either upward or downward frequency chirping that the mode would exhibit as a consequence of adiabatically slow changes in the local q profile. Here, by adiabatically slow we mean on characteristic time scales which are much longer than the inverse mode growth rate. In this sense, all equilibrium quantities are treated as ''fixed'' parameters; the parametrized model prediction (mode frequency and growth rate), in turn, would adiabatically depend on time through the corresponding slow time changes of the plasma equilibrium under investigation.[5–7]

Using the physical argument of spatial scale separation between equilibrium quantities and mode wavelengths, we have shown that there exists a unified mathematical formulation, which is valid both for vanishing magnetic shear near r_0 and in the region inside the minimum-q surface, where magnetic shear is small but finite. On the basis of this unified formulation, we have argued that most unstable EPMs are generally excited at the radial position of strongest energetic particle drive.

The linear theory developed here allows us to define excitation thresholds for both EPM gap modes and resonant EPMs. Our results are consistent with experimental observations of Alfvén cascades.[6–9] However, it also suggests that a richer phenomenology can be observed by suitable choices of experimental conditions. Acting on density of the minority ion species or on the position of the ICRH resonant absorption layer provides direct control on the velocity ratio v_{TH}/v_A, which has a crucial role in determining the compressional response of the fast ion population, e.g., by setting the value of $\Omega = \Omega_0(v_{TH}/v_A, \ldots)$, where $\mathbb{R}\mathrm{e}\,\Lambda_m(\Omega)$ vanishes. For $-\Omega_{A,m} < \Omega_{A,m-1} < \Omega_0$, a drop in q_0, due to current diffusion, results in upwards frequency chirping of the EPM gap mode at r_0, as it is observed with Alfvén cascades. However, for $\Omega_0 < -\Omega_{A,m} < \Omega_{A,m-1}$, the direction of chirping would be downwards, and, even further, both upwards and downwards chirping modes should be observed for $-\Omega_{A,m} < \Omega_0 < \Omega_{A,m-1}$. This prediction of the present theory can be easily checked in actual experimental conditions.

Adjusting the position of the ICRH resonant absorption layer or changing the level of power input provides an experimental knob for regulating the power density and, ultimately, the strength of energetic particle drive. In this way, it is possible to control a smooth transition from EPM gap modes to resonant EPM excitation. Unlike EPM gap modes, that are readily observed with magnetic fluctuation measurements at the plasma edge, direct detection of resonant EPMs requires radially resolved fluctuation measurements.

For sufficiently peaked pressure profiles, nonlinear simulations confirm that resonant EPMs are destabilized at the radial location where α_H is maximum. Numerical results show that nonlinearly saturated states are always characterized by EPM gap modes at the minimum-q surface, even when EPMs of either type are excited within the minimum-q surface. Scenarii that yield these time-''asymptotic'' saturated conditions continuously vary between two limiting cases. Close to marginal stability, the transport time scale of energetic ions is longer than the inverse growth rate of both resonant EPMs and EPM gap modes excited at r_0. In these conditions, EPM excitations at different radial locations are well described within the theoretical formulations of Secs. II and III, and the modes are characterized by independent nonlinear evolutions. For strong drive, rapidly evolving resonant EPMs are radially displacing the fast ion source towards the position where it can more easily destabilize more weakly growing EPM gap modes. In this second case, the characteristic time scale of EPM gap mode growth is longer than that

of fast ion transport: linear stability analyses are, thus, inadequate and the problem is intrinsically nonlinear.

The presence of an EPM gap mode at the minimum-q surface in both limiting scenarii, as well as in the case in which resonant EPMs are not excited, makes spectrographic measurements of frequency spectra at the plasma edge not suited for discriminating among the various cases, which are characterized by crucial differences in nonlinear fast ion dynamics. More information could be obtained by searching evidence of resonant EPMs within the minimum-q surface in radially resolved fluctuation spectra, e.g., based on reflectometry. Detection of the resonant EPMs would indicate that experimental conditions can be appropriately described in terms of a *close to marginal stability* regime. On the other hand, lack of evidence of these resonant modes could be interpreted, on the basis of numerical results, in two opposite ways: (i) complete absence of EPMs excited within the minimum-q surface; (ii) strongly unstable EPMs and rapid energetic particle transport that yields mode saturation. This uncertainty can be obviously removed by direct detection of fast frequency chirping of strongly excited EPMs within the minimum-q surface during their nonlinear saturation process. However, such measurement is difficult and is a challenge for realistic reflectometry time resolution, since it involves characteristic times that scale as the inverse mode growth rate and are shorter than any ''equilibrium'' relaxation time.[3] Fast reflectometry with time resolution shorter that 1 ms would be required to actually resolve rapid frequency chirping in the early nonlinear phase of strongly unstable resonant EPMs. If this were not available, only nonlinearly saturated mode structures would be detected. Indirect evidence of strong resonant EPM excitation can, however, be obtained by observing that actually measured energetic particle profiles are significantly broader than those expected from power deposition calculations. Such discrepancy, according to simulation results, could be explained in terms of EPM-induced fast ion transport.[34]

From the present work, linear stability aspects seem to be fairly well understood. However, the issue of nonlinear EPM dynamics and fast ion transport requires further analyses, as far as both numerical simulations and theoretical modeling are concerned. In fact, fast ion distributions and radial profiles may be of crucial importance in determining which operation scenarii are accessible in present and next step experiments. The expected radial profiles of energetic ions would be quite different depending on whether or not resonant EPMs are excited within the minimum-q surface. Nonetheless, in the presence of external ion heating (ICRH, NBI, N-NBI), the usually adopted approach is to compute fast ion distributions treating them as test particles. In other words, the possibility that collective phenomena may be excited and eventually cause fast ion transport is neglected. This classic approach is inadequate in burning plasma conditions or with high power-density additional heating and the effect of collective phenomena, as EPMs, should be self-consistently included.

Our numerical simulations of EPM induced fast ion transports so far have been made using simplifying assumptions on fast ion distribution (isotropic Maxwellian) and plasma equilibria (shifted circular magnetic surfaces).[11,12,19,20,25] Their main ''robust'' results are essentially that rapid fast ion transport occurs right above the excitation threshold of resonant EPMs, but that—at the same time—the nature of such transport (local radial redistributions vs global losses) depends on the details of radial mode structures, fast ion profiles and plasma equilibrium (essentially the q profile). As a consequence, if remaining everywhere below the local excitation threshold of resonant EPMs is an obvious and elementary criterion for plasma operations, locally unstable fast ion profiles can be acceptable, especially for peaked energetic particle sources that are only likely to cause radially trapped modes and local radial redistributions.[3] With peaked fast ion profiles, the nonlinear saturated EPM can also induce localized zonal flows in the plasma, although the effect that these may have on core transport remains to be assessed.[36,37] Thus, it is of primary importance to develop reliable theoretical models of fast ion transport in the presence of resonant EPMs as well as predictive numerical simulation capabilities.

In this work, we have focused on the fundamental physics aspects of EPM excitation and mode structure in tokamaks with hollow q profiles, rather than on applications and comparisons with actual experimental conditions. The present results on mode stability, summarized by Eqs. (16) and (B5)–(B8), may indeed be taken as the starting point for further work with the aim of designing experimental setups in which specific aspects of wave and particle dynamics could be studied. The fairly simple and compact form of the equations could be used to rapidly obtain preliminary and useful results for more detailed and complex numerical investigations.[7] Similar consideration can obviously be made for nonlinear simulations using the HMGC code.[11,12]

ACKNOWLEDGMENTS

This work was partly supported by UCI U.S. Department of Energy Contract No. DE-FG03-94ER54271 and MIT U.S. Department of Energy Contract No. DE-FG02-99ER54563, and was conducted partly under the European Fusion Development Agreement. The JET data presented was partly obtained under the framework of the JET Joint Undertaking.

APPENDIX A: EPM MODE STRUCTURES: NONLOCAL CONTINUUM DAMPING

In this section, we take a closer look at Eq. (1) in order to compute the *nonlocal continuum damping* associated with the nonlocal interaction with the shear Alfvén continuous spectrum as shown in Fig. 1. Introducing the new variable $y \equiv n^{1/2} x/S$, it is straightforwardly seen that the eigenvalue problem for the (m,n) mode—the one that can be *localized* by the *negative* fast ion compressibility, as indicated in Eq. (3)—reduces to an asymptotic matching between two regions: I, characterized by $x \approx 1 \Leftrightarrow Sy/\sqrt{n} \approx 1$, in which

$$\left[\partial_y^2-1+\frac{2/y}{(1+S^2y^2/4n\Omega_{A,m})}\partial_y + \frac{S^2}{n\Omega_{A,m}}\frac{y\partial_y}{(1+S^2y^2/4n\Omega_{A,m})} + \frac{n\Lambda_m/S^2\Omega_{A,m}}{y^2(1+S^2y^2/4n\Omega_{A,m})}\right]\delta\psi_m=0; \tag{A1}$$

and II, where $x\ll 1\Leftrightarrow Sy/\sqrt{n}\ll 1$ and

$$\left[\partial_y^2-1+\frac{2yS^2/n\partial_y}{(2(\Omega+\Omega_{A,m})+S^2y^2/n)}\partial_y + \frac{\Lambda_m/\Omega_{A,m}}{(2(\Omega+\Omega_{A,m})+S^2y^2/n)}\right]\delta\psi_m=0. \tag{A2}$$

Using the symmetry of Eqs. (A1) and (A2) for $y\rightarrow -y$, we may focus on the $y\geqslant 0$ axis. Equation (A1) is evidently the one that contains the *nonlocal* interaction with the shear Alfvén continuous spectrum (see Fig. 1) in the singular points at $y^2=y_0^2\equiv -4n\Omega_{A,m}/S^2$. Omitting the lengthy but straightforward details, it is possible to show that Eq. (A1) has the following solution for $y\rightarrow y_0^{(+)}$:

$$\delta\psi_{m,I}^{(+)}\simeq(y^2|y_0^2-y^2|)^{-1/2}\sqrt{|y-y_0|}K_0(y-y_0), \tag{A3}$$

where K_0 is the modified Bessel function of zero order. Equation (A3) has the correct asymptotic behavior for $y\gg y_0$, i.e., $\delta\psi_{m,I}^{(+)}\simeq\sqrt{\pi/2}\exp(y_0-y)/y^2$. Using the *causality constraints* to analytically continue the solution of Eq. (A3) across $y=y_0$, i.e., to describe the mode interaction with the shear Alfvén continuous spectrum,[38] we have that Eq. (A1) has the following solution for $y\rightarrow y_0^{(-)}$:

$$\delta\psi_{m,I}^{(-)}\simeq(y^2|y_0^2-y^2|)^{-1/2}\sqrt{|y-y_0|} \times[K_0(y_0-y)+i\pi I_0(y_0-y)]. \tag{A4}$$

For $1\ll y\ll y_0$, Eq. (A4) yields $\delta\psi_{m,I}^{(-)}\simeq i\sqrt{\pi/2}(\exp y_0/y)\times(\exp(-y)-i\exp(-2y_0)\exp(y))$, which must match the asymptotic solution of Eq. (A2). In fact, this condition may be actually used as a boundary condition for the solution of Eq. (A2) as $y\gg 1$. At this point, the eigenvalue problem is well posed and, proceeding as in Ref. 3, we find the dispersion relation for the *even* mode, i.e., Eq. (4):

$$\sqrt{\Omega_{A,m}+\Omega}[1+i\exp(-4\sqrt{-n\Omega_{A,m}}/S)] = \frac{S\pi}{2^{5/2}n^{1/2}}\left(\frac{2n}{S^2}\frac{\Lambda_m}{\Omega_{A,m}}-1\right).$$

Equation (4) is the generalization of Eq. (3) that includes the effect of the *nonlocal* continuum damping, which is exponentially small and depends on the mode frequency, via $\Omega_{A,m}$, as it was expected from Fig. 1. The trend is that of an exponential reduction of *nonlocal* continuum damping as the mode frequency increases. We emphasize again that, in our opinion, this is the reason why EPMs in reversed shear discharges on JET appear only above a certain minimum mode frequency[5,6] (see Fig. 2, from Ref. 5).

APPENDIX B: TOROIDAL DISPERSION RELATION AND MODE STRUCTURES

When $\Omega_{A,m}+\Omega_{A,m-1}\geqslant r_0/R_0$, (m,n) and $(m-1,n)$ modes can be considered independent because of the weak (perturbative) influence of toroidal coupling. This effect cannot be treated as a perturbation anymore as $\Omega_{A,m}+\Omega_{A,m-1}\rightarrow 0$, as it clearly emerges from Fig. 3.

Assume that $\Omega_{A,m}\simeq -\Omega_{A,m-1}\simeq -1/2$. At this value of $\Omega_{A,m}$, the effect of *nonlocal* continuum damping becomes exponentially small (cf. Appendix A). Thus, we will omit its explicit computation in the toroidal case. In these conditions, the most relevant damping mechanism is *radiative damping*[15,16] or *ion Landau damping*,[17] that could be straightforwardly included in the present formalism.[4] However, for the sake of simplicity, we will neglect these damping mechanisms in the present analysis to better emphasize the novel and peculiar features in the mode structures of toroidal Alfvénic modes near a minimum-q surface.

Equation (1) in Fourier space is replaced by[3]

$$\left[\partial_{\kappa_r}(1+\kappa_r^2)\partial_{\kappa_r}+\frac{\Omega^2-\Omega_{A,m}^2}{\Theta_m}(1+\kappa_r^2)+\frac{\Lambda_m}{\Theta_m}\right]\delta\phi_m + \frac{\epsilon_0\Omega^2}{\Theta_m}\kappa_r^2\delta\phi_{m-1}=0,$$
$$\left[\partial_{\kappa_r}(1+\kappa_r^2)\partial_{\kappa_r}+\frac{\Omega^2-\Omega_{A,m-1}^2}{\Theta_{m-1}}(1+\kappa_r^2)+\frac{\Lambda_{m-1}}{\Theta_{m-1}}\frac{n}{S^2}\right]\delta\phi_{m-1} + \frac{\epsilon_0\Omega^2}{\Theta_{m-1}}\kappa_r^2\delta\phi_m=0. \tag{B1}$$

Here, Θ_m is the same that was defined in Eq. (14). Meanwhile, κ_r is the Fourier conjugate variable of $m(r-r_0)/r_0$, introduced above in Sec. III, whereas $\delta\phi_m,\delta\phi_{m-1}$ are the Fourier Transforms of $\delta\psi_m,\delta\psi_{m-1}$. Introduce also the notation $\Gamma_m=(\Omega^2-\Omega_{A,m}^2)/\Theta_m$, and $E_m=-\epsilon_0\Omega^2/\Theta_m\simeq -E_{m-1}$. Taking into account that $\Theta_{m-1}\simeq-\Theta_m$, it is readily demonstrated[3,5] that the asymptotic solution of Eq. (B1) for $\kappa_r\gg 1$ is given by

$$\delta\phi_m\simeq\frac{1}{2\kappa_r}\left[c_+\left(\sqrt{\frac{\Gamma_m-\Gamma_{m-1}}{2}+E_m}+\sqrt{\frac{\Gamma_m-\Gamma_{m-1}}{2}-E_m}\right)\exp i(k_+\kappa_r) + c_-\left(\sqrt{\frac{\Gamma_m-\Gamma_{m-1}}{2}+E_m}-\sqrt{\frac{\Gamma_m-\Gamma_{m-1}}{2}-E_m}\right)\exp i(k_-\kappa_r)\right], \tag{B2}$$

$$\delta\phi_{m-1}\simeq\frac{1}{2\kappa_r}\left[c_+\left(\sqrt{\frac{\Gamma_m-\Gamma_{m-1}}{2}+E_m}-\sqrt{\frac{\Gamma_m-\Gamma_{m-1}}{2}-E_m}\right)\exp i(k_+\kappa_r)\right.$$
$$\left.+c_-\left(\sqrt{\frac{\Gamma_m-\Gamma_{m-1}}{2}+E_m}+\sqrt{\frac{\Gamma_m-\Gamma_{m-1}}{2}-E_m}\right)\exp i(k_-\kappa_r)\right], \tag{B3}$$

where $c_\pm$ are arbitrary constants and

$$k_\pm^2=\frac{\Gamma_m+\Gamma_{m-1}}{2}\pm\sqrt{\left(\frac{\Gamma_m-\Gamma_{m-1}}{2}\right)^2-E_m^2}. \tag{B4}$$

Clearly, $k_\pm$ are defined as the roots of Eq. (B4) with $\mathbb{I}\mathrm{m}\,k_\pm>0$.

As for the ''cylindrical'' case (see Sec. II), Eqs. (B1) can be used to generate a variational form, in which Eqs. (B2) and (B3) can be used as trial functions. Considering that $\Lambda_m\simeq\Lambda_{m-1}$, this lengthy but straightforward calculation yields the following dispersion relation for toroidal EPMs near a minimum-q surface:

$$\left[\sqrt{E_m^2+\Gamma_m\Gamma_{m-1}}+\frac{\pi^2}{16}-i\frac{\pi}{4}(k_++k_-)\right.$$
$$\left.-\left(\frac{\pi\Lambda_m}{2\Theta_m}\right)^2\right](k_++k_-)=i\frac{\pi\Lambda_m}{2\Theta_m}(\Gamma_m-\Gamma_{m-1}). \tag{B5}$$

It is instructive to consider a simple limit of the above equation in which the effect of toroidicity may be neglected. Assuming $\Gamma_m\Gamma_{m-1}\gg E_m^2$, Eq. (B4) gives

$$\begin{aligned}&k_++k_-=i\sqrt{-\Gamma_m}+i\sqrt{-\Gamma_{m-1}},\\&k_+-k_-=\mathrm{sgn}(\Gamma_m-\Gamma_{m-1})(i\sqrt{-\Gamma_m}-i\sqrt{-\Gamma_{m-1}}).\end{aligned} \tag{B6}$$

With these results, Eq. (B5) becomes

$$\left(\sqrt{-\Gamma_m}+\frac{\pi}{4}-\frac{\pi\Lambda_m}{2\Theta_m}\right)\left(\sqrt{-\Gamma_{m-1}}+\frac{\pi}{4}+\frac{\pi\Lambda_m}{2\Theta_m}\right)=0, \tag{B7}$$

i.e., it recovers the cylindrical limit of Eq. (16).

In general, Eq. (B5) requires a numerical solution, despite its fairly simple and compact form that, as we just showed, can describe consistently the toroidal mode dispersion relation as well as the cylindrical limit. However, there is a simple but still relevant toroidal case in which Eq. (B5) can be cast into a more transparent form. This is the case when either the toroidal EPM gap modes or the toroidal resonant EPMs have a frequency very close to the accumulation point of the shear Alfvén continuous spectrum and $\Gamma_{m-1}=-\Gamma_m$, i.e., $\Omega_{A,m}=-\Omega_{A,m-1}=-1/2$. Then, with the optimal ordering

$$(E_m^2-\Gamma_m^2)^{1/4}\approx\left|\frac{\pi\Lambda_m}{2\Theta_m}\mp1\right|\approx\epsilon_0^{1/2},$$

we readily obtain the dispersion relation for the toroidal mode, Eq. (9), as anticipated in Sec. II:

$$[\epsilon_0^2\Omega^4-(\Omega^2-1/4)^2]^{1/4}$$
$$=-\frac{S\pi}{8n^{1/2}}\left[\left(1\pm4\frac{n\Lambda_m}{S^2}\right)\right.$$
$$\left.+\mathrm{sgn}(\cdot)\sqrt{\left(1\pm4\frac{n\Lambda_m}{S^2}\right)^2+\frac{16\epsilon_0 n}{\pi^2S^2}}\right],$$
$$\mathrm{sgn}(\cdot)=\mathrm{sgn}\,\mathbb{R}\mathrm{e}\left(1\pm4\frac{n\Lambda_m}{S^2}\right).$$

Here, the upper (lower) sign refers to an EPM mode excited near the lower (upper) accumulation point of the shear Alfvén continuum, i.e., $\Omega^2\simeq(1/4)(1\mp\epsilon_0)$.

On the left-hand side of Eq. (9), the expression $[\epsilon_0^2\Omega^4-(\Omega^2-1/4)^2]$, which accounts for the toroidal frequency gap formation in the shear Alfvén continuous spectrum, is the same that appears in the well-known case with finite magnetic shear, $q_0'\neq0$. The difference, here, is that this expression enters the equation at the 1/4 power, rather than the square root: this is due to the peculiar structure of the shear Alfvén continuous spectrum in the present case, with four (rather than two) shear Alfvén waves that are degenerate at the lowest order.

For $\mathbb{R}\mathrm{e}(1+4n\Lambda_m/S^2)<0$, and considering that $\mathbb{I}\mathrm{m}\,\Lambda_m<0$ (cf. Appendix C), it is readily demonstrated that the upper sign corresponds to an EPM gap mode excited at $\Omega^2\simeq(1/4)(1-\epsilon_0)$, whereas no gap mode may exist for the lower sign. On the contrary, for $\mathbb{R}\mathrm{e}(1-4n\Lambda_m/S^2)<0$, an EPM gap mode is excited at $\Omega^2\simeq(1/4)(1+\epsilon_0)$ (lower sign), but no gap mode may be located near the lower continuum accumulation point (upper sign). Actually, Eq. (9) gives only the most unstable modes that may be excited in the conditions described above. Two other roots are possible as well, i.e., those given by Eq. (10),

$$[\epsilon_0^2\Omega^4-(\Omega^2-1/4)^2]^{1/4}$$
$$=-\frac{S\pi}{8n^{1/2}}\left[\left(1\pm4\frac{n\Lambda_m}{S^2}\right)\right.$$
$$\left.-\mathrm{sgn}(\cdot)\sqrt{\left(1\pm4\frac{n\Lambda_m}{S^2}\right)^2+\frac{16\epsilon_0 n}{\pi^2S^2}}\right].$$

For $\mathbb{R}\mathrm{e}(1+4n\Lambda_m/S^2)<0$, the lower sign gives an EPM gap mode excited near the upper continuum accumulation point, which is characterized by a much weaker drive than that of the EPM gap mode at $\Omega^2\simeq(1/4)(1-\epsilon_0)$, described by Eq. (9). Similarly, for $\mathbb{R}\mathrm{e}(1-4n\Lambda_m/S^2)<0$, Eq. (10) yields a much weaker EPM gap mode at $\Omega^2\simeq(1/4)(1-\epsilon_0)$ (upper sign) than that of Eq. (9), located near the upper accumulation point (lower sign).

One effect of toroidal coupling is, thus, to increase the number of unstable modes: these are indeed two, rather than one as in the ''cylindrical case,'' at least in the conditions discussed above for the validity of Eqs. (9) and (10). However, Eq. (B5) shows clearly that no toroidal gap modes can exist in the absence of fast ions, i.e., $\Lambda_m=0$, since $\mathbb{I}\mathrm{m}(k_+ + k_-)>0$. This result is evidently an artifact of the intrinsic assumption made in this Appendix: that thermal (core) plasma compression is negligible with respect to that of the fast ions. In fact, this assumption is reasonable in the presence of ion cyclotron resonant heating (ICRH). But it evidently fails if we wish to take the $\Lambda_m\to 0$ limit in Eq. (B5). Following Ref. 3, the effect of core plasma compressibility is readily included into Eqs. (B1) and (B5). Omitting the details of the derivation for brevity, we directly write the generalization of Eq. (B5),

$$\left[\sqrt{E_m^2+\Gamma_m\Gamma_{m-1}}+\frac{\pi^2}{16}-i\frac{\pi}{4}(k_++k_-)-\left(\frac{\pi\Lambda_m}{2\Theta_m}\right)^2 + \left(\frac{\pi(\alpha-\alpha_{c0})}{4\Theta_m}\right)^2\right](k_++k_-) = i\frac{\pi\Lambda_m}{2\Theta_m}(\Gamma_m-\Gamma_{m-1})+iE_m\frac{\pi(\alpha-\alpha_{c0})}{2\Theta_m}, \tag{B8}$$

where $\alpha=-R_0q^2\beta'$ and $\alpha_{c0}=r_0/R_0+2\Delta'$.[3,29] Equation (B8), similarly to Eq. (B5), generally requires a numerical solution. However, it admits a very simple solution near the continuum accumulation points and with $\Lambda_m=0$,

$$[\epsilon_0^2\Omega^4-(\Omega^2-1/4)^2]^{1/4}=\frac{4\sqrt{2}}{\pi}\frac{n^{3/2}}{S^3}\epsilon_0(\alpha_{c0}-\alpha). \tag{B9}$$

Equation (B9) demonstrates that toroidal Alfvén eigenmodes[10] exist at a minimum-q surface, provided $\alpha<\alpha_{c0}$, even in the absence of a fast ion population.

APPENDIX C: FAST ION RESONANT AND NONRESONANT RESPONSE

In this appendix, we derive an expression for Λ_m in Eq. (1), i.e., for the wave-particle resonant and nonresonant interactions. Here, it is worth noticing that fast ions orbits produced during ion cyclotron resonant heating may well be nonconventional *potato* orbits.[39] These potato orbits are characterized by a typical width, δ_p, comparable with the mode radial localization, i.e., $\delta_p\approx r_0$. For such particles, the characteristic orbit size normalized to the poloidal wavelength is $(m/r_0)\delta_p\approx m\gg 1$, and their interaction with high-m localized modes is affected by strong *resonance detuning*.[1,3,4,40] On the other hand, some potato orbits may not reach $\theta=\pi/2$ in poloidal angle (the typical bounce angle for trapped particles with *on axis* ICRH), depending on the value of their toroidal canonical angular momentum. However, these orbits do not effectively tap energy from the ICRH since they do not reach the resonant absorption layer. Thus, orbits that most effectively exchange energy with high-m modes tend to be conventional trapped *banana* orbits. For this reason, and since transition from potato to banana orbits can be obtained by changing (lowering) the particle energy,[39] in the following we will assume that ICRH heated ions that effectively exchange energy with EPMs are characterized by conventional banana orbits. For *fat* banana orbits, in the high energy transition region to potato orbits, this assumption obviously fails, but the error in evaluating the resonant energy exchange would be nonetheless small because, as stated above, $(m/r_0)\delta_p\approx m\gg 1$. In what follows we will also see that this assumption is appropriate not only for the *resonant* but also for the *nonresonant* wave-particle interactions even for a case with $\bar{\omega}_{dH}\gtrsim\omega_{BH}\gg\omega$, ω_{BH} being the fast ion bounce frequency between magnetic mirror points. In fact, in this *very energetic particle* limit, the nonresonant fast-ion response in not sensitive to the details of the drift orbits.

For the reasons discussed above, we may closely follow the analysis of Ref. 3, which solves the fast ion gyrokinetic equations for *deeply trapped* particles [Eqs. (2)–(10) therein]. Thus, for the particle distribution function we assume the representation[41,42]

$$\delta f_H=\left(\frac{e}{m}\right)_H\left[\frac{\partial F_{0H}}{\partial v^2/2}\delta\phi-J_0(\lambda_H)\frac{QF_{0H}}{\omega}e^{iL_{kH}}\delta\psi\right] + e^{iL_{kH}}\delta K_H, \tag{C1}$$

where $\delta\phi$ is the perturbed scalar potential and $\delta\psi$ is related to the perturbed parallel vector potential as $\mathbf{b}\cdot\nabla\delta\psi\equiv-(1/c)\partial_t\delta A_\parallel$. Furthermore, $L_{kH}=(\mathbf{k}\times\mathbf{b})\cdot\mathbf{v}/\omega_{cH}$ and δK_H is obtained from the following gyrokinetic equation for the energetic ions:[42]

$$[v_\parallel\mathbf{b}\cdot\nabla-i(\omega-\omega_{dH})]\delta K_H=i\frac{e_H}{m_H}QF_{0H}J_0(\lambda_H)\frac{\omega_{dH}}{\omega}\delta\psi. \tag{C2}$$

For *deeply trapped* banana orbits, we have that the particles' bounce motion between magnetic mirror points (located at $\theta=\pm\theta_b$) is given by $v_\parallel\simeq\theta_bqR_0\omega_{BH}\cos\eta$, with the bounce frequency given by $\omega_{BH}=[(v^2/2)(r/R_0)]^{1/2}/qR_0$ and

$$\omega_{dH}\simeq\bar{\omega}_{dH}(1+\theta_b\xi\sin\eta), \tag{C3}$$

where $\xi\equiv(i/m)r\partial/\partial r$ is to be intended as a differential operator and the toroidal precession frequency is $\bar{\omega}_{dH}=(v^2/2)\times(m/r)/(\omega_{cH}R_0)$. Transforming to the banana orbit center frame,[40] we have

$$\delta K_H=\left(\sum_h i^hJ_h(\lambda_{BH})e^{-ih\eta}\right)\delta K_{BH},$$

where $\lambda_{BH}\equiv\theta_b(\bar{\omega}_{dH}/\omega_{BH})\xi$ and the banana orbit distribution function, δK_{BH}, satisfies the following gyrokinetic equation:[3]

$$[\omega_{BH}\partial_\eta-i(\omega-\bar{\omega}_{dH})]\delta K_{BH} = i\frac{e_H}{m_H}QF_{0H}\sum_h(-i)^he^{ih\eta}J_0(\lambda_H)J_h(\lambda_{BH}) \times\left(1+h\frac{\theta_b\xi}{\lambda_{BH}}\right)\frac{\bar{\omega}_{dH}}{\omega}\delta\psi. \tag{C4}$$

Note that, for a correct interpretation of Eq. (C4), the deeply trapped particle assumption has to be kept in mind. If not, inconsistencies would arise on the way $\delta\psi$ appears on the

right-hand side. Within this framework, Eq. (C4) is easily integrated and the (magnetic) flux surface averaged contribution of fast ions can be obtained in the form[3]

$$\Lambda_m \simeq -\frac{q^2R_0^2}{m^2/r_0^2}\left(\frac{r_0}{R_0}\right)^{1/2} v_{TH}^3 \frac{8}{\pi}\int_0^\infty \frac{dz}{1+z^2}\int_0^\infty w^{1/2}\,dw \times \int_0^\pi d\theta_b \sin\theta_b \mathbf{K}(\sin(\theta_b/2))\frac{4\pi\omega}{c^2}\frac{e_H^2}{m_H}J_0^2(\lambda_H)QF_{0H} \times \sum_h J_h^2(\lambda_{BH})\frac{\bar{\omega}_{dH}+h\omega_{BH}}{\bar{\omega}_{dH}+h\omega_{BH}-\omega}, \quad \text{(C5)}$$

where $\mathbf{K}(\sin(\theta_b/2))$ is the complete elliptic integral of the first kind, $v_{TH}\equiv\sqrt{T_H/m_H}$ is the fast tail ion thermal speed, $w\equiv v^2/2v_{TH}^2$, $\lambda_H=\sqrt{2w}k_\theta\rho_{LH}\sqrt{1+z^2}$, $\rho_{LH}=v_{TH}/\omega_{cH}$, $\lambda_{BH}=\sqrt{wR_0/r_0}\theta_b z q_0 k_\theta\rho_{LH}$, $\bar{\omega}_{dH}=k_\theta\rho_{LH}(v_{TH}/R_0)w$, and $\omega_{BH}=\sqrt{wr_0/R_0}(v_{TH}/q_0R_0)$.

The expression of Λ_m from Eq. (C5) is made of two contributions:[3] the *positive compression* term associated with the convective response, i.e., the second term on the right-hand side of Eq. (C1); and the resonant plus nonresonant response coming from δK_H in the same equation. The positive compression term is that which yields the usual fast ion *ballooning-interchange* drive[3] and it is always associated with a *downwards* frequency shift. The $\propto\delta K_H$ fast ion compressions, instead, depend crucially on the details of the particle equilibrium distribution function and, as a consequence, on the detailed particle dynamics, including particle orbits. In particular, the *nonresonant* (real) part of such response may change sign as either the fast ion energy, e.g., via v_{TH}/v_A, or the parallel wave vector are changed. Here, parallel wave vector or mode frequency may be equally used, since $qR_0\omega/v_A\simeq\pm(nq-m)\simeq qR_0k_\parallel$. In the very energetic ion limit, $\bar{\omega}_{dH}\gg\omega$, the fast ion compression $\propto\delta K_H$ becomes negative and it cancels the positive compression term to the lowest order in $(\omega/\bar{\omega}_{dH})$. It may be interesting to note that the same result is valid assuming a *flute-like* limit, i.e., $qR_0k_\parallel\simeq\Omega\to 0$. This digression should put the emphasis on the fact that the type of nonresonant particle response depends both on the details of the particle dynamics (distribution function) and on the mode structure. From the experimental point of view, these are the properties that must be controlled in order to explore the various regimes corresponding to fundamental changes in the dynamic properties of the system.

The nonresonant contribution of energetic ions from Eq. (C5) clearly reduces to the expression of Eq. (2) for $\bar{\omega}_{dH}\gg\omega$, keeping into account that $\Sigma_h J_h^2=1$ and that, for deeply trapped particles, the flux surface averaged value of the velocity space integral is

$$\overline{\langle(\cdots)\rangle}=4\left(\frac{r_0}{R_0}\right)^{1/2} v_{TH}^3\int_0^\infty w^{1/2}\,dw\int_0^\pi d\theta_b\sin\theta_b \times\mathbf{K}(\sin(\theta_b/2))(\cdots).$$

Thus, as mentioned above, the property of Eq. (2) to predict $\Lambda_m<0$ is strictly connected with the properties of the particle orbits at $\bar{\omega}_{dH}\gg\omega$. Note that this fact, as it was discussed in the previous section, is what *selects* which of the two branches described by Eq. (3) is excited. $\Lambda_m<0$ is obviously compatible with the excitation of localized modes just above the local maximum of the shear Alfvén continuous spectrum of the (m,n) mode (cf. Fig. 1). The opposite case would instead yield the excitation of a localized mode just below the local minimum of the shear Alfvén continuous spectrum of the $(m-1,n)$ mode. Thus, in the former case, a drop in the value of q_0 (as observed experimentally[5–7]), would manifest itself as an *upward frequency chirping*, whereas in the second case a *downward frequency chirping* mode would be predicted, the critical control parameter between the two situations being the sign of Λ_m, i.e., a quantity determined by fast ion dynamics and, ultimately, by the properties of fast ion distribution function. In fact, the present results could be used to design experimental operation scenarii for switching from one situation to the other by simply controlling the fast ion tail energy, e.g., acting on the density of the minority ion species. Evidently, only a conceptual experiment could be so flexible to operate in all possible scenarii that are interesting from the theoretical point of view. But changing the additional heating scheme, e.g., to NBI (or N–NBI[35] as mentioned in the Introduction), would introduce additional flexibility in controlling the particle distribution function and, ultimately, the fast ion compressional response.

[1] L. Chen, Phys. Plasmas **1**, 1519 (1994).
[2] L.-J. Zheng, L. Chen, and R. A. Santoro, Phys. Plasmas **7**, 2469 (2000).
[3] F. Zonca and L. Chen, Phys. Plasmas **7**, 4600 (2000).
[4] F. Zonca and L. Chen, Phys. Plasmas **3**, 323 (1996).
[5] D. Testa, F. Zonca, S. Briguglio, L. Chen, S. Dettrick, G. Vlad, A. Fasoli, A. Gondhalekar, and contributors to the EFDA-JET work programme, European Conference Abstracts **25A**, 489 (2001). Also in CD-ROM *Proceedings of Contributed Papers, 28th EPS Conference on Controlled Fusion and Plasma Physics*, Madeira, Portugal, 2001, edited by C. Silva, C. Varandas, and D. Campbell (European Physical Society, Petit-Lancy, 2001).
[6] H. L. Berk, D. N. Borba, B. N. Breizman, S. D. Pinches, and S. E. Sharapov, Phys. Rev. Lett. **87**, 185002 (2001).
[7] D. Borba, H. L. Berk, B. N. Breizman *et al.*, "Modelling of Alfvén waves in JET plasmas with the CASTOR-K code," in *Proceedings of Contributed Papers, 7th IAEA Tech. Comm. Meet. on Energetic Particles in Magnetic Confinement Systems, Goteborg, Sweden, 2001* (International Atomic Energy Agency, Vienna, to be published). Available online at http://www.elmagn.chalmers.se/tcm/it11.pdf
[8] S. E. Sharapov, D. Testa, B. Alper *et al.*, Phys. Lett. A **289**, 127 (2001).
[9] S. E. Sharapov (private communication).
[10] C. Z. Cheng, L. Chen, and M. S. Chance, Ann. Phys. (N.Y.) **161**, 21 (1985).
[11] S. Briguglio, G. Vlad, F. Zonca, and C. Kar, Phys. Plasmas **2**, 3711 (1995).
[12] S. Briguglio, F. Zonca, and G. Vlad, Phys. Plasmas **5**, 3287 (1998).
[13] K. Appert, R. Gruber, F. Troyon, and J. Vaclavik, Plasma Phys. **24**, 1147 (1982).
[14] J. P. Goedbloed, Physica D **12**, 107 (1984).
[15] N. N. Gorelenkov and S. E. Sharapov, Phys. Scr. **45**, 163 (1992).
[16] R. R. Mett and S. M. Mahajan, Phys. Fluids B **4**, 2885 (1992).
[17] R. Betti and J. P. Freidberg, Phys. Fluids B **4**, 1465 (1992).
[18] F. Zonca, Ph.D. thesis, Princeton University, Plasma Physics Laboratory, Princeton, NJ, 1993.
[19] S. Briguglio, G. Vlad, F. Zonca, and D. Testa, "Particle-in-cell investigation of the nonlinear saturation of shear Alfvén modes in hollow-q-profile tokamaks," *Proceedings of Contributed Papers, 7th IAEA Technical Communications Meeting on Energetic Particles in Magnetic Confinement Systems, Goteborg, Sweden, 2001* (International Atomic Energy Agency, Vienna, to be published). Available online at http://www.elmagn.chalmers.se/tcm/ot9.pdf

[20]S. Briguglio, G. Vlad, F. Zonca, and G. Fogaccia, Phys. Lett. A **302**, 308 (2002).
[21]J. W. Connor, R. J. Hastie, and J. B. Taylor, Phys. Rev. Lett. **40**, 396 (1978).
[22]F. Zonca and L. Chen, Phys. Fluids B **5**, 3668 (1993).
[23]D. Testa, W. G. F. Core, and A. Gondhalekar, Phys. Plasmas **6**, 3489 (1999).
[24]D. Testa, W. G. F. Core, and A. Gondhalekar, Phys. Plasmas **6**, 3498 (1999).
[25]G. Vlad, F. Zonca, and S. Briguglio, Riv. Nuovo Cimento **22**, 1 (1999).
[26]L. Chen, in *Theory of Fusion Plasmas*, edited by J. Vaclavik, F. Troyon, and E. Sindoni (Editrice Compositori, Bologna, 1989), p. 327.
[27]C. Z. Cheng, G. Fu, and J. V. Dam, in *Theory of Fusion Plasmas*, edited by J. Vaclavik, F. Troyon, and E. Sindoni (Editrice Compositori, Bologna, 1989), p. 259.
[28]G. Y. Fu and C. Cheng, Phys. Fluids B **2**, 985 (1990).
[29]G. Y. Fu, Phys. Plasmas **2**, 1029 (1995).
[30]B. N. Breizman and S. E. Sharapov, Plasma Phys. Controlled Fusion **37**, 1057 (1995).
[31]H. L. Berk, J. W. V. Dam, D. Borba, J. Candy, G. T. A. Huysmans, and S. Sharapov, Phys. Plasmas **2**, 3401 (1995).
[32]E. D. Fredrickson, M. G. Bell, R. V. Budny *et al.*, Nucl. Fusion **35**, 1457 (1995).
[33]S. Bernabei, M. G. Bell, R. V. Budny *et al.*, Phys. Plasmas **6**, 1880 (1999).
[34]G. Vlad, S. Briguglio, G. Fogaccia, and F. Zonca, European Conference Abstracts 26B, P4.088 (2002), *Nonlinear Dynamics of Shear Alfvén Modes and Energetic Ion Confinement in Optimized Shear Tokamak Equilibria*. To be published in CD-ROM *Proceedings of Contributed Papers, 29th EPS Conference on Controlled Fusion and Plasma Physics, Montreux, Switzerland, 2002* (European Physical Society, Petit-Lancy, 2002).
[35]K. Shinohara, Y. Kusama, M. Takechi *et al.*, Nucl. Fusion **41**, 603 (2001).
[36]F. Zonca, S. Briguglio, L. Chen, G. Fogaccia, and G. Vlad, ''Theoretical aspects of collective mode excitations by energetic ions in tokamaks,'' in *Theory of Fusion Plasmas*, edited by J. W. Connor, O. Sauter, and E. Sindoni (Editrice Compositori, Bologna, 2000), pp. 17–30.
[37]F. Zonca, S. Briguglio, L. Chen, G. Fogaccia, G. Vlad, and L.-J. Zheng, *Energetic Particle Modes Dynamics in Tokamaks*, IAEA Fusion Energy 2000, 18th Conference Proceedings, Sorrento, Italy, 2000 (IAEA, Vienna, Austria, 2001), IAEA-CSP-8/C, Paper THP2/20.
[38]L. Chen and A. Hasegawa, Phys. Fluids **17**, 1399 (1974).
[39]L.-G. Eriksson and F. Porcelli, Plasma Phys. Controlled Fusion **43**, R145 (2001).
[40]S. T. Tsai and L. Chen, Phys. Fluids B **5**, 3284 (1993).
[41]T. M. Antonsen and B. Lane, Phys. Fluids **23**, 1205 (1980).
[42]L. Chen and A. Hasegawa, J. Geophys. Res., [Solid Earth] **96**, 1503 (1991).